Ferroelectric nanotraps for polar molecules

Omjyoti Dutta[1] and G. Giedke[1,2]
[1]*IKERBASQUE, Basque Foundation for Science, 48013 Bilbao, Spain*
[2]*Donostia International Physics Center, 20018 San Sebastián, Spain*

(Received 3 November 2017; published 16 February 2018)

We propose and analyze an electrostatic-optical nanoscale trap for cold diatomic polar molecules. The main ingredient of our proposal is a square array of ferroelectric nanorods with alternating polarization. We show that, in contrast to electrostatic traps using the linear Stark effect, a quadratic Stark potential supports long-lived trapped states. The molecules are kept at a fixed height from the nanorods by a standing-wave optical dipole trap. For the molecules and materials considered, we find nanotraps with trap frequency up to 1 MHz, ground-state width ∼20 nm with lattice periodicity of ∼200 nm. Analyzing the loss mechanisms due to nonadiabaticity, surface-induced radiative transitions, and laser-induced transitions, we show the existence of trapped states with lifetime ∼1 s, competitive with current traps created via optical mechanisms. As an application we extend our discussion to a one-dimensional (1D) array of nanotraps to simulate a long-range spin Hamiltonian in our structure.

DOI: 10.1103/PhysRevA.97.023416

I. INTRODUCTION

Ultracold atoms and molecules trapped in optical potentials constitute a versatile toolbox for simulating a plethora of Hamiltonians [1]. The energy scale for such trapping is set by the optical wavelength and laser strength. To go beyond this energy scale, there is a recent surge in investigations of trapping atoms in subwavelength lattices. Most of these studies concentrate on hybrid atom-dielectric systems and the use of vacuum forces to achieve lattice constants on the order of ∼50 nm [2,3]. Naturally, a pertinent question in this regard is to extend such trapping schemes for polar molecules, which because of their rich internal structure and potentially strong interactions have raised considerable interest as a basis for quantum computation and simulation [4–6]. Additionally, the presence of a permanent dipolar moment in such molecules is responsible for a plethora of exotic physics with applications in quantum engineering [7–10] and precision measurements [11]. The use of a nanoscale trap can be beneficial for these applications because of its increased energy scale. For a comparison, in typical optical lattices ($\lambda \sim 1.06\ \mu$m) with a microwave-coupled RbCs molecule, the maximum nearest-neighbor interaction energy is on the order of ∼0.5 kHz (30 nK). Since the dipolar interaction falls off as a cubic power of distance and a threefold decrease in lattice constant will result in a 27-fold increase of interaction strength. This energy scale can potentially give rise to $\sim 10^4$ gate operations, within a typical molecule lifetime of ∼1 s, for quantum information processing applications. Another advantageous consequence of nanoscale confinement originates from the reduced tunneling and overlap between neighboring sites, a possible mechanism for suppression of molecular complex formation [12]. We propose a setup to create a subwavelength trap for cold rovibrational ground-state polar molecules which are prepared, e.g., in optical lattices [13,14]. Ferroelectric materials can provide a natural basis for such traps. Nanoscale ferroelectricity is a source of intense research because of its potential application as nonvolatile memories, sensors, etc. [15]. It has been found that monodomain ferroelectricity survives for nanorods with radius down to ∼20 nm [16–18]. Taking advantage of state-of-art lithography and nanotechnology [19–25] techniques, it is possible to create a periodic array of ferroelectric nanorods. Moreover, using cantilever tips or external loads, polarization of each nanocell can also be controlled externally [26,27]. This enables, in principle, the design of potential landscapes to trap polar molecules.

In this paper, we propose an electrostatic-optical trap for rigid-rotor $^1\Sigma$ diatomic polar molecules. The subwavelength trap is provided by the electric field created by a periodic arrangement of ferroelectric nanorods. An optical potential is used to prevent the molecules from moving away from the nanostructure. We show that it is possible to obtain a nanometer-sized trap for molecules in high-field-seeking states with a lifetime on the order of seconds. Such lifetime is achieved by the virtue of two ingredients: (i) the existence of a trapped state with negligible nonadabatic (Majorana) loss and (ii) the suppression of additional losses due to hyperfine mixing by applying a strong magnetic field on the order of a few Tesla for 1D trapping.

At this point, we like to stress that trapping molecules using electrostatic force has a long history [28]. In most of these studies, the molecules are trapped using linear Stark shift. Such traps suffer from Majorana losses near the trap center owing to their kinetic origin [29]. Therefore, reducing the trap size to the nanometer (nm) regime in general will make the molecules extremely short-lived (lifetime on the order of few microseconds or less). In our proposal, the trapping potential originates as a second-order perturbative effect (quadratic Stark shift). By analyzing the quantum motion, we show the presence of motional states in which the nonadiabatic coupling is weakened considerably by destructive interference. Additionally, we discuss molecule loss due to both vacuum photons and thermal phonons in the presence of a substrate. We finish the article by a proposal to simulate a long-range XX spin Hamiltonian.

The paper is arranged as follows: We present the hyperfine and rotational structure of a $^1\Sigma$ molecule in Sec. II; in particular, we consider ^{87}Rb^{133}Cs (RbCs) as a paradigmatic example. In Sec. III, we present our ferroelectric structure corresponding to a 0D arrangement of nanorods. Section IV contains a detailed analysis of the 0D electric field and its trapped states. In Sec. V, we close the trap in the Z direction by adding a suitable laser field. Additionally, we sketch a method for electrostatically trapping the general molecules. The main loss mechanisms (nonadiabatic and hyperfine-induced losses and losses due to nanostructure and laser field) are discussed and shown to be small in Secs. VI and VII. Sections VIII and IX consider the extension to a 1D system and propose a quantum simulator using our traps.

II. MOLECULAR HAMILTONIAN

Here we consider a rigid-rotor $^1\Sigma$ diatomic molecule amenable to laser cooling. The molecular Hamiltonian in the electronic and vibrational ground state is given by [30]

$$\begin{aligned} H_{\rm mol} &= \hbar B_e \boldsymbol{N}^2 + \sum_i c_i \boldsymbol{I}_i \cdot \boldsymbol{N} + c_4 \boldsymbol{I}_1 \cdot \boldsymbol{I}_2 + H_{\rm Q} + H_{\rm mag}, \\ H_{\rm Q} &= \frac{\sum_i (eqQ)_i \left[3(\boldsymbol{I}_i \cdot \boldsymbol{N})^2 + \frac{3}{2}(\boldsymbol{I}_i \cdot \boldsymbol{N}) - \boldsymbol{N}^2 \boldsymbol{I}_i^2\right]}{2\mathcal{I}_i(2\mathcal{I}_i - 1)(2\mathcal{N} - 1)(2\mathcal{N} + 3)}, \\ H_{\rm mag} &= -g_r \mu_{\rm N} \boldsymbol{N} \cdot \vec{B} - \mu_{\rm N} \sum_i g_i (1 - \sigma_i) \boldsymbol{I}_i \cdot \vec{B}, \end{aligned} \tag{1}$$

where the first term gives the rotational spectrum where $\boldsymbol{N}$ is the total angular momentum operator and B_e is the rotational constant. The second term takes into account interaction of the rotational angular momentum with the nuclear spins and the third term denotes the direct interaction between the nuclear spins. As we are interested in diatomic molecules, the total nuclear spin operators of the two atoms are denoted by $\boldsymbol{I}_{1,2}$. The Hamiltonian $H_{\rm Q}$ denotes quadrupole interaction with coupling constants $(eqQ)_{1,2}$. The last term in the Hamiltonian denotes the Zeeman term in the presence of a magnetic field $\vec{B}$ where g_r is the rotational g factor of the molecule and $g_{1,2}$ are the nuclear g factors with typically $g_{1,2} \gg g_r$. In the present paper, we apply a magnetic field along the Z direction, $\vec{B} = B_0 \hat{Z}$. A full description of the internal molecular state is then denoted by $|\mathcal{N},\mathcal{M}_\mathcal{N},\mathcal{I}_1,\mathcal{M}_{\mathcal{I}_1},\mathcal{I}_2,\mathcal{M}_{\mathcal{I}_1}\rangle$, where, $\boldsymbol{N}^2|\mathcal{N},\mathcal{M}_\mathcal{N}\rangle = \mathcal{N}(\mathcal{N}+1)|\mathcal{N},\mathcal{M}_\mathcal{N}\rangle, \boldsymbol{N}_Z|\mathcal{N},\mathcal{M}_\mathcal{N}\rangle = \mathcal{M}_\mathcal{N}|\mathcal{N},\mathcal{M}_\mathcal{N}\rangle$, $\mathcal{N} \in [0,1,2,\dots], -\mathcal{N} \geqslant \mathcal{M}_\mathcal{N} \geqslant \mathcal{N}$ and the same for the nuclear spin operators.

As a first step, we diagonalize the Hamiltonian in Eq. (1) for the ^{87}Rb^{133}Cs molecule ($\mathcal{I}_1 = \mathcal{I}_{\rm Cs} = 7/2, \mathcal{I}_2 = \mathcal{I}_{\rm Rb} = 3/2$). The hyperfine constants are taken from Ref. [31]. We are especially interested in the rotational levels $\mathcal{N} = 1, \mathcal{M}_\mathcal{N} = \pm 1$. This justification for choosing such state will be clarified in Sec. IV. Moreover, for the present purpose we ignore coupling to the $\mathcal{N} = 1, \mathcal{M}_\mathcal{N} = 0$ state, which can be detuned by application of laser fields (see Sec. V A). For concreteness, we chose the magnetic field $B = B_0$ such that the two lowest energy states are almost degenerate. These states are

$$\begin{aligned} |\alpha_0\rangle &= |1,1,7/2,3/2\rangle, \\ |\beta_0\rangle &\approx (1 - \delta^2/2)\,|1,-1,7/2,3/2\rangle - \delta\,|1,1,7/2,-1/2\rangle, \end{aligned} \tag{2}$$

where $\delta \ll 1$, and $|\alpha_0\rangle$ is the maximally polarized state which has no quadrupolar coupling. On the other hand, the $|1,-1,7/2,3/2\rangle$ state is coupled to $|1,1,7/2,-1/2\rangle$ via $H_{\rm Q}$. Without the magnetic field, such coupling will lead to an equal superposition of these states. Moreover, the $H_{\rm mol}$ eigenvalues for the states $|\alpha_0\rangle$, $|\beta_0\rangle$ are $\approx 2\hbar B_e - E_0 - \Delta_{\rm hf}/2$, and $\approx 2\hbar B_e - E_0 + \Delta_{\rm hf}/2$, where E_0 is the energy and $\Delta_{\rm hf}$ is the detuning due to hyperfine and Zeeman Hamiltonian of Eq. (1).

For future use (see Sec. IV), we will also consider the energy eigenstates in which $|1,\pm 1,7/2,-1/2\rangle$ has the majority contribution:

$$\begin{aligned} |\alpha_1\rangle &\approx \left(1 - \delta^2/2 - \delta_1^2/2\right)|1,1,7/2,-1/2\rangle + \delta_1 |1,1,5/2,1/2\rangle \\ &\quad + \delta |1,-1,7/2,3/2\rangle, \\ |\beta_1\rangle &\approx \left(1 - \delta_1^2/2\right)|1,-1,7/2,-1/2\rangle + \delta_1 |1,-1,5/2,1/2\rangle, \end{aligned} \tag{3}$$

where $\delta_1 \ll 1$ and $|\alpha_1\rangle$, $|\beta_1\rangle$ are $H_{\rm mol}$ eigenstates with eigenenergies $2\hbar B_e - E_1 - \Delta_{\rm hf}/2 \approx 2\hbar B_e - E_1 + \Delta_{\rm hf}/2$, where E_1 is the energy contribution from the hyperfine and Zeeman Hamiltonian. In Sec. IV, we will see that these states are coupled to $|\alpha_0\rangle$, $|\beta_0\rangle$ by the electric field of the ferroelectric rods. For future use, we introduce a shorthand notation for the nuclear spin quantum numbers by the collective symbol, $\mathcal{I}_{\rm col} \equiv \{\mathcal{I}_{\rm Cs}, \mathcal{M}_{\mathcal{I}_{\rm Cs}}, \mathcal{I}_{\rm Rb}, \mathcal{M}_{\mathcal{I}_{\rm Rb}}\}$, and as a result a general state is written as

$$|\mathcal{N},\mathcal{M}_\mathcal{N},\mathcal{I}_{\rm col}\rangle \equiv \left|\mathcal{N},\mathcal{M}_\mathcal{N},\mathcal{I}_1,\mathcal{M}_{\mathcal{I}_1},\mathcal{I}_2,\mathcal{M}_{\mathcal{I}_1}\right\rangle. \tag{4}$$

III. POLAR MOLECULES NEAR 0D FERROELECTRIC NANOSTRUCTURES

Our system consists of a symmetric arrangement of polarized ferroelectric nanorods. The elementary structure consists of four cylindrical nanorods centered around each corner of a square as shown in Fig. 1(a). Each nanorod has a radius $r_{\rm d}$ and height $h \geqslant r_{\rm d}$. Within a cell, neighboring nanorods are separated by a distance a_d. The unit vectors $\hat{X}$ and $\hat{Y}$ along the plane of the cell are shown in the second panel of Fig. 1(a). We measure Z from the top surface of the nanorods and denote the centers of the four rods by $(m_x, m_y)a_d/2 \equiv \vec{F}_{\mathbf{m}}, m_i = \pm 1$, respectively. We consider an antiferroelectric arrangement where polarization of each rod is given by $P_{\mathbf{m}} = (-1)^{(m_x+m_y)/2} P$. From now on, we scale all distances by the nanorod radius $r_{\rm d}$ unless otherwise explicitly specified. In this paper, such nanorod arrangement is referred to as 0D structure.

We study polar molecules near such ferroelectric nanostructures. In general, our model Hamiltonian is given by $H_{\rm sys} = H_{\rm kin} + H_{\rm mol} + H_{\rm mf}$, where $H_{\rm kin}$ is the kinetic energy of the center of mass of the molecule, $H_{\rm mol}$ is given in Eq. (1) and $H_{\rm mf}$ denotes the interaction between a single molecule and a nanostructured cylinder.

A. Molecule-ferroelectric interaction

First, we set the notation for the molecular position as $\rho = (\vec{R}, Z)$, where the transverse vector $\vec{R} \equiv (X, Y)$. The

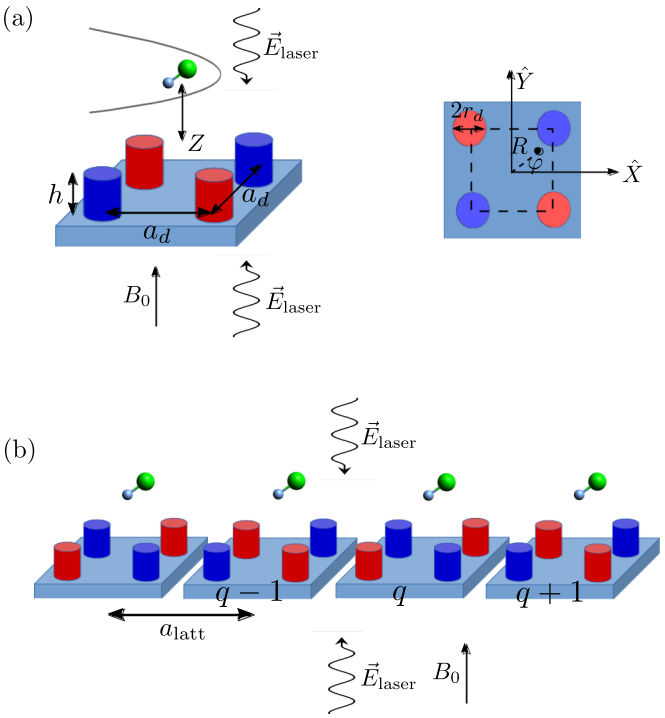

FIG. 1. (a) Left panel: Side view of our primitive cell is shown. Each nanorod is made of ferroelectric material. The red and blue colors of the rods denote the $\pm\hat{Z}$ direction of the ferroelectric polarization, respectively. We place a dipolar molecule at a height Z above the top of the nanorods. We illuminate the system by counterpropagating optical laser fields, which provide a trap for the molecule along the Z direction. Moreover, we apply a static magnetic field $B_0\hat{Z}$ to minimize hyperfine loss. Right panel: Top view of our primitive cell. We define the local polar coordinate system. (b) We arrange the primitive cells periodically along the X axis. Notice the $\pi/2$ rotation of the ferroelectric arrangement between neighboring cells. The periodicity of the cells is denoted by $a_{\rm latt}$.

molecule-ferroelectric interaction is given by the dipole Hamiltonian and expressed as

$$H_{\rm mf} = -\alpha_{\rm mf}\left[E_Z[\vec{\rho}]\boldsymbol{T}^1_{\boldsymbol{0}} + E_-[\vec{\rho}]\frac{\boldsymbol{T}^1_{\boldsymbol{1}}}{\sqrt{2}} + E_+[\vec{\rho}]\frac{\boldsymbol{T}^1_{\boldsymbol{-1}}}{\sqrt{2}}\right], \quad (5)$$

where $\boldsymbol{T}^1_0 = \cos\theta_{\rm in}$, $\boldsymbol{T}^1_{\pm1} = \sin\theta_{\rm in}e^{\pm i\phi_{\rm in}}/\sqrt{2}$ are the spherical tensors of rank 1 denoting the internal coordinates of the molecule and only act on the rotational states $|\mathcal{N},\mathcal{M}_\mathcal{N}\rangle$. The molecular axis in the laboratory frame is defined by the angles to the Z axis and its projection to the X axis, $\theta_{\rm in},\phi_{\rm in}$. Here, $E_Z[\vec{\rho}]$ is the Z component of the electric field and $E_\pm[\vec{\rho}] = (E_X[\vec{\rho}] \pm i\,E_Y[\vec{\rho}])$ are its azimuthal components. We should note that electric fields are dimensionless in our units. We define the effective molecule-ferroelectric coupling strength, $\alpha_{\rm mf} = \frac{\mu P}{4\pi\epsilon_0}$, where μ is the permanent dipole moment of the molecule. For RbCs molecules, the dipole moment is given by $\mu = 1.22$ Debye [32].

After carrying out integration over the height of the nanorods, the field strength at $\vec{\rho}$ due to the ferroelectric nanorod at position $(m_x a_d, m_y a_d)$ reads

$$\begin{aligned} E_Z[\boldsymbol{m};\vec{\rho}] &= -\int d\vec{r}(ZE[Z] - (Z+h)E[Z+h]), \\ E_-[\boldsymbol{m};\vec{\rho}] &= -e^{-i\tilde{\phi}_{\boldsymbol{m}}}\int d\vec{r}(E[Z+h] - E[Z]) \\ &\quad \times (R_{\boldsymbol{m}} - re^{-i(\phi-\phi_{\boldsymbol{m}})}), \\ E[Z] &= \frac{1}{(Z^2 + |\vec{R}_{\mathbf{m}} - \vec{r}|^2)^{3/2}}, \end{aligned} \quad (6)$$

where $\vec{R}_{\boldsymbol{m}} = \vec{R} - \vec{F}_{\boldsymbol{m}}$, $\boldsymbol{m} \equiv (m_x,m_y)$ and $\tan\phi_{\boldsymbol{m}} = (Y - m_y a_d)/(X - m_x a_d)$ and we have defined a local polar coordinate around each nanorod axis $\vec{r} \equiv (r,\phi)$. The integral is defined as $\int d\vec{r} = \int_0^1 r dr \int_0^{2\pi} d\phi$. The total field components are given as the sum of the contributions of all nanorods by $E_Z[\vec{\rho}], E_-[\vec{\rho}]$:

$$E_\eta[\vec{\rho}] = \sum_{\boldsymbol{m}}(-1)^{\frac{m_x+m_y}{2}}E_\eta[\boldsymbol{m};\vec{\rho}] \ (\eta = Z,-). \quad (7)$$

For the azimuthal electric fields, $E_+[\vec{\rho}] = E^*_-[\vec{\rho}]$. From the expression in Eq. (6), it is clear that each ferroelectric nanorod can be effectively substituted by opposite surface charges at the top and bottom of the nanorods.

To treat the effect of ferroelectric nanorods on the molecular motion and identify the trap provided by the proposed arrangement, we operate in a regime with $\alpha_{\rm mf}|E_\pm[\vec{\rho}]|, \alpha_{\rm mf}|E_Z[\vec{\rho}]| \ll \hbar B_e$, which allows us to carry out a second-order perturbation analysis for each $\mathcal{N}$ manifold. Note that selection rules imply that $\langle\mathcal{N}|\,H_{\rm mf}\,|\mathcal{N}'\rangle \propto \delta_{\mathcal{N}',\mathcal{N}\pm1}$. Moreover, we neglect the detuning effect of hyperfine splitting as $c_{1,2},c_4,(eqQ)_{1,2},\mu_{\rm N}B_0 \ll B_e$ and suppress the hyperfine structures of the molecular state in the notation. From the Hamiltonians in Eqs. (1) and (5), we derive an effective potential of the form

$$\begin{aligned} V^{\mathcal{N}} = \frac{\alpha^2_{\rm mf}}{2\hbar B_e}\big(&E_+[\vec{\rho}]E_-[\vec{\rho}]V^{\mathcal{N}}_\perp + E^2_-[\vec{\rho}]V^{\mathcal{N}}_+ + E^2_+[\vec{\rho}]V^{\mathcal{N}}_- \\ &+ E^2_Z[\vec{\rho}]V^{\mathcal{N}}_Z + E_Z[\vec{\rho}]E_-[\vec{\rho}]V^{\mathcal{N}}_{Z+} + E_Z[\vec{\rho}]E_+[\vec{\rho}]V^{\mathcal{N}}_{Z-}\big), \end{aligned} \quad (8)$$

where $V^{\mathcal{N}}_- = [V^{\mathcal{N}}_+]^\dagger, V^{\mathcal{N}}_{Z-} = [V^{\mathcal{N}}_{Z+}]^\dagger$ and

$$\begin{aligned} V^{\mathcal{N}}_\perp &= \sum_{\eta=\pm1}\sum_{\mathcal{N}',\mathcal{M}_{\mathcal{N}'}}\frac{\boldsymbol{T}^1_\eta\,|\mathcal{N}',\mathcal{M}_{\mathcal{N}'}\rangle\langle\mathcal{N}',\mathcal{M}_{\mathcal{N}'}|\,\boldsymbol{T}^1_{-\eta}}{E_\mathcal{N} - E_{\mathcal{N}'}}, \\ V^{\mathcal{N}}_+ &= \sum_{\mathcal{N}',\mathcal{M}_{\mathcal{N}'}}\frac{\boldsymbol{T}^1_{\boldsymbol{1}}\,|\mathcal{N}',\mathcal{M}_{\mathcal{N}'}\rangle\langle\mathcal{N}',\mathcal{M}_{\mathcal{N}'}|\,\boldsymbol{T}^1_{\boldsymbol{1}}}{E_\mathcal{N} - E_{\mathcal{N}'}}, \\ V^{\mathcal{N}}_Z &= \sum_{\mathcal{N}',\mathcal{M}_{\mathcal{N}'}}\frac{\boldsymbol{T}^1_{\boldsymbol{0}}\,|\mathcal{N}',\mathcal{M}_{\mathcal{N}'}\rangle\langle\mathcal{N}',\mathcal{M}_{\mathcal{N}'}|\,\boldsymbol{T}^1_{\boldsymbol{0}}}{E_\mathcal{N} - E_{\mathcal{N}'}}, \\ V^{\mathcal{N}}_{Z+} &= \sum_{\substack{\eta,\eta'=0,1\\ \eta\neq\eta'}}\sum_{\mathcal{N}',\mathcal{M}_{\mathcal{N}'}}\frac{\boldsymbol{T}^1_\eta\,|\mathcal{N}',\mathcal{M}_{\mathcal{N}'}\rangle\langle\mathcal{N}',\mathcal{M}_{\mathcal{N}'}|\,\boldsymbol{T}^1_{\eta'}}{E_\mathcal{N} - E_{\mathcal{N}'}}. \end{aligned} \quad (9)$$

While deriving Eq. (8), we have made the assumption that the molecular center-of-mass motion is adiabatic; i.e., it is slow compared to the rotational splitting. In Appendix B, we discuss the nonadiabatic corrections to this approximation.

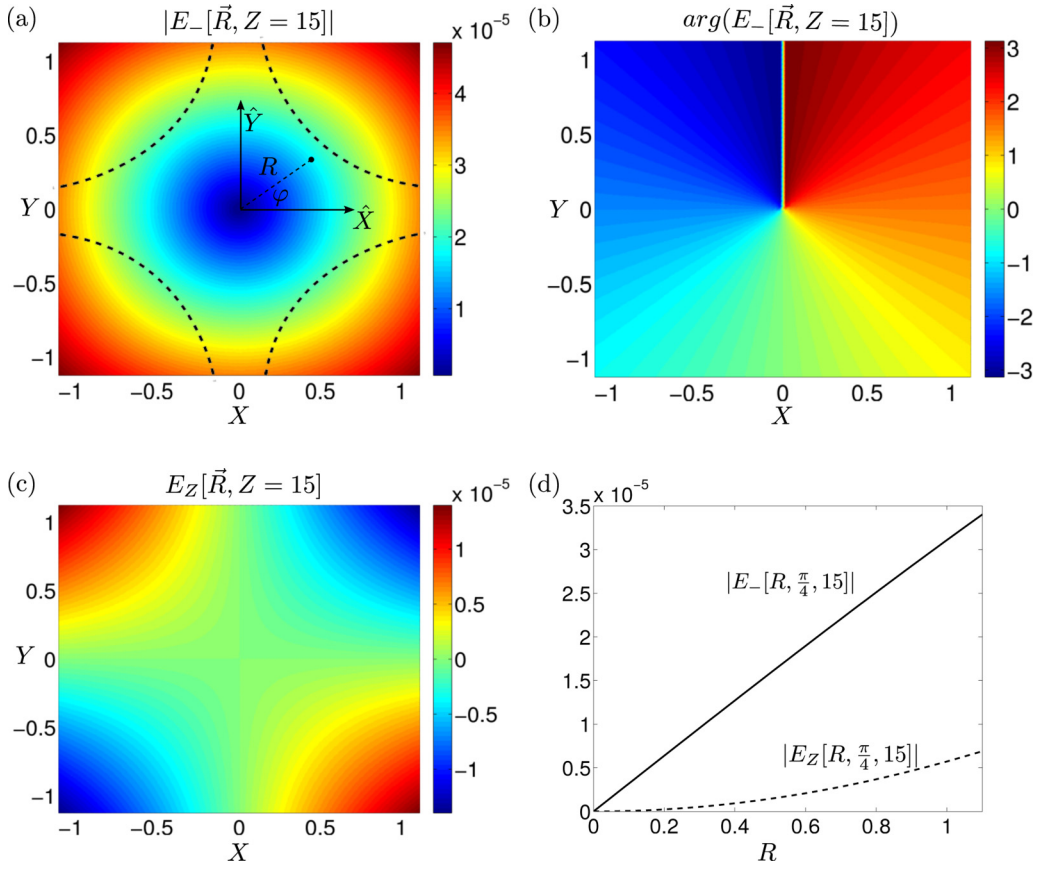

FIG. 2. Electric field distribution of the 0D nanorods arrangement as in Fig. 1 with $N_f = 0$ and $a_d = 2.25$. (a) The magnitude of the azimuthal field distribution $E_-[\vec{\rho}]$ in the XY plane is shown for $Z = 15$. At the center of the square, the electric field vanishes due to the reflection and $\pi/2$ rotational symmetries. Moreover, we define a local polar coordinate from the center of each square: (R,φ). For $R \lesssim 1$, the $E_|\vec{\rho}]$ field magnitude grows linearly with R. The black dashed lines denote boundaries of the nanorods along the XY plane. (b) The argument of $E_-[\vec{\rho}]$ is shown. We clearly see that in terms of the local polar coordinate, $E_-[\vec{\rho}] \approx ie^{i\varphi}$. (c) The field distribution of E_Z is plotted. The Z field has maximum magnitude along the two diagonals and has a angular distribution $\propto \sin 2\varphi$. (d) $|E_-[\vec{\rho}], E_Z[\vec{\rho}]|$ are plotted as a function of distance along the diagonal from the center.

IV. 0D NANOTRAPS FOR MOLECULES

First, we investigate the simplest ferroelectric geometry consisting of only four nanorods; i.e., the 0D structure introduced above, cf. Fig. 1. As we shall see, this configuration can laterally confine molecules in a suitable internal state to the center of the arrangement; hence we call it a 0D nanotrap. To obtain this result, we consider the form of the electric field at the center of the square. We can gain useful insights from symmetry arguments: The field sources change orientation under rotation (around the Z axis) by $\pi/2$ as well as under reflections either at $Y = 0$ or at $X = 0$. This constrains the Fourier series of the azimuthal field component (written using in-plane polar coordinates R,φ, collectively referred to as $\vec{R}$) $E_-(\varphi,R,Z) = \sum_l c_l(R,Z)e^{il\varphi}$ (cf. Appendix A): Only the coefficients c_l with $l = 4j + 1$ may be nonzero and they are imaginary and odd functions of R. Specifically, we have that $c_{-1}[R,Z] = c_3[R,Z] = 0$.

Moreover, note that as the electric field is nonsingular, we have in general that $c_n[R,Z] \propto R^n$ as $R \to 0$. Thus, $c_1[R,Z] \propto R$ for small R. For the Z components, we can similarly show that it contains only even powers of R and by Gauss's law $\nabla \cdot \vec{E} = 0$ we have $E_Z[\varphi,R,Z] \propto O[R^2]$ for small R. Such electric fields resemble a traditional quadrupolar field configuration. For illustration purposes, we plot the field distributions in Fig. 2. In Figs. 2(a) and 2(b) amplitude and argument of the azimuthal field is shown. For $R < a_d/2$, we indeed notice that $E_-[\vec{\rho}] \propto ie^{i\varphi}$. The linear dependence of $E_-[\vec{\rho}]$ with R is clearly seen in Fig. 2(d) as is the angular dependence of $E_Z[\vec{\rho}]$ in Eq. (10) in Fig. 2(c). Moreover, $E_Z[\vec{\rho}]$ depends quadratically on R to the leading order as can be verified from Fig. 2(d).

Thus we find for small R for the field given in Eq. (7) that

$$\begin{aligned} E_-[\vec{\rho}] &\approx iR(f_\perp[a_d,Z] + f_{1\perp}[a_d,Z]R^2)\exp[i\varphi] \\ &\quad + if_{-3}[a_d,Z]\exp[-3i\varphi]R^3 + O[R^5], \\ E_Z[\vec{\rho}] &\approx f_z[a_d,Z]R^2\sin[2\varphi] + O[R^4], \end{aligned} \tag{10}$$

where Gauss's law leads to the form of $E_Z[\vec{\rho}]$ with $\partial_Z f_z[a_d,Z] - 3(2f_{1\perp}[a_d,Z] + f_{-3}[a_d,Z]) = 0$. We use $f_\perp[a_d,Z], f_{1\perp}[a_d,Z], f_{-3}[a_d,Z]$ as fitting functions which we obtain numerically and which are shown in Fig. 3. It is clear that the largest parameter is $f_\perp[a_d,Z]$, corresponding to the linear dependence of the azimuthal electric field with R as $f_{1\perp}[a_d,Z]/f_\perp[a_d,Z] \sim 10^{-2}$, and $f_{-3}[a_d,Z]/f_\perp[a_d,Z] \sim 5.0 \times 10^{-3}$. Moreover, we see that

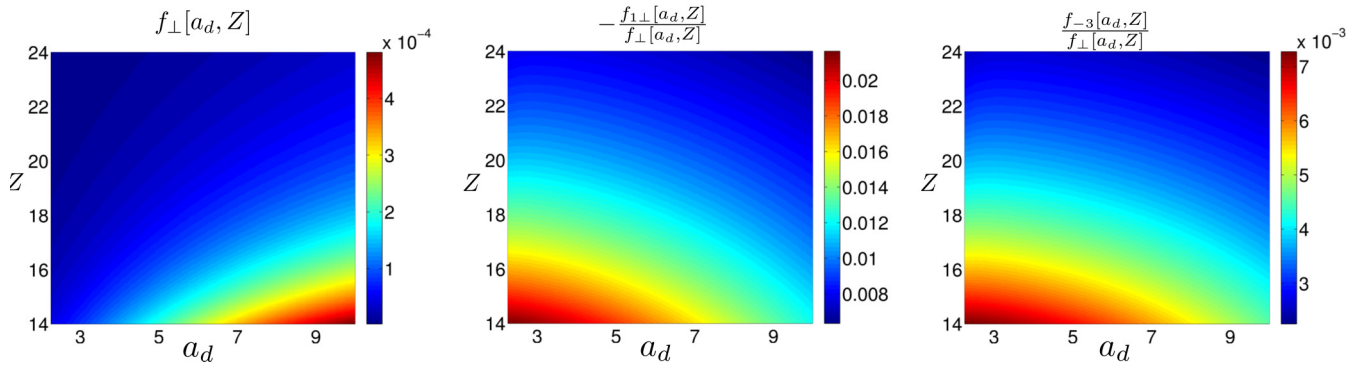

FIG. 3. We plot the fitting functions in Eq. (10) as a function of a_d and Z. Left panel, $f_\perp[a_d,Z]$; middle panel, $-f_{1\perp}[a_d,Z]/f_\perp[a_d,Z]$; and right panel, $f_{-3}[a_d,Z]/f_\perp[a_d,Z]$.

by increasing the lattice constant one increases $f_\perp[a_d,Z]$ and simultaneously one decreases the relative strength of the fitting functions associated with R^3 scaling, whereas by increasing Z, we see a decrease in each fitting function due to the scaling of the dipolar interaction.

As the electric fields vanish as $R \to 0$, we can write the effect of the ferroelectric nanorods within perturbation theory as presented in Eq. (8). We consider the first excited rotational level $\mathcal{N} = 1$ manifold with $\mathcal{M}_1 = \pm 1$. The $\mathcal{M}_\mathcal{N} = 0$ state is excluded from further consideration due to its large shift in energy from the $\mathcal{M}_\mathcal{N} = \pm 1$ as will be shown later. Moreover, for $R < a_d/2$, the $E_\pm[\vec{\rho}]$ field components are dominant compared to $E_Z[\vec{\rho}]$, which is then neglected at first. Subsequently we only keep the $V^1_\perp, V^1_\pm$ from Eq. (8). Using the state description of Eq. (4), we find that the effective potential is

$$V^1_{\rm rad} = \frac{f^2_\perp[a_d,Z]\alpha^2_{\rm mf}}{40\hbar B_e} R^2 \sum_{\substack{\mathcal{M}_1=\pm1 \\ \mathcal{I}_{\rm col}}} \big(|1,\mathcal{M}_1,\mathcal{I}_{\rm col}\rangle \langle 1,\mathcal{M}_1,\mathcal{I}_{\rm col}| - 3e^{2i\mathcal{M}_1\varphi}|1,\mathcal{M}_1,\mathcal{I}_{\rm col}\rangle\langle 1,-\mathcal{M}_1,\mathcal{I}_{\rm col}|\big), \tag{11}$$

where we have used the expression for $E_\pm[\vec{\rho}]$ from Eq. (10), retaining the leading term $\propto R$. By inspecting Eq. (11), it is clear that for each $\mathcal{I}_{\rm col}$ a trapped state can be formed by the superposition:

$$|-,\varphi\rangle \equiv \sum_{\mathcal{M}_1=\pm1} |1,\mathcal{M}_1,\mathcal{I}_{\rm col}\rangle\, e^{i\mathcal{M}_1\varphi}/\sqrt{2}. \tag{12}$$

We are now ready to consider the joint effect of the internal Hamiltonian $H_{\rm mol}$ in Eq. (1) and the effective potential in Eq. (11). Specifically, we will transform to the diagonal basis of $H_{\rm mol}$ and consider the states $|\alpha_{0,1}\rangle$, $|\beta_{0,1}\rangle$ in Eqs. (2) and (3).

Exploiting the approximate cylindrical symmetry of our problem, we write down explicitly the position dependence of individual internal states as $\langle \vec{R} \mid \alpha_j\rangle = \sum_\ell a^j_\ell[R]e^{-i\ell\varphi}/\sqrt{2\pi}$ and $\langle \vec{R} \mid \beta_j\rangle = \sum_\ell b^j_\ell[R]e^{-i\ell\varphi}/\sqrt{2\pi}$, where $j = 0,1$ denotes the molecular internal state and $\ell = 0, \pm 1, \pm 2, \ldots$ represents the center-of-mass angular momentum around the laboratory Z axis. Additionally, for the time being, we neglect motion of the particle along the Z axis (see Sec. V A) and as a result the Z dependence is implicit in the coefficients. We use the transformed coefficients $t^j_\ell[R] = (a^j_\ell[R] - b^j_{\ell-2}[R])/\sqrt{2}, u_\ell[R] = (a^j_\ell[R] + b^j_{\ell-2}[R])/\sqrt{2}$. Moreover, to simplify the notation, we introduce the array $\boldsymbol{t}^j_\ell[R] = [t^j_\ell[R]\ u^j_\ell[R]]^T$. In terms of the transformed coefficients, the Schrödinger equation in closed form reads

$$\begin{bmatrix} H_{00} & H_{01} \\ H_{10} & H_{11} \end{bmatrix} \begin{bmatrix} \boldsymbol{t}^0_\ell[R] \\ \boldsymbol{t}^1_{\ell-2}[R] \end{bmatrix} = \epsilon \begin{bmatrix} \boldsymbol{t}^0_\ell[R] \\ \boldsymbol{t}^1_{\ell-2}[R] \end{bmatrix}, \tag{13}$$

where the matrices are given by

$$H_{00} = \begin{bmatrix} -K\left(\partial^2_R + \frac{\partial_R}{R} - \frac{(\ell-1)^2+1}{R^2}\right) + \frac{(f_\perp[a_d,Z]\alpha_{\rm mf})^2R^2}{10\hbar B_e} - E_0 & 2K\frac{\ell-1}{R^2} - \frac{\Delta_{\rm hf}}{2} \\ 2K\frac{\ell-1}{R^2} - \frac{\Delta_{\rm hf}}{2} & -K\left(\partial^2_R + \frac{\partial_R}{R} - \frac{(\ell-1)^2+1}{R^2}\right) - \frac{(f_\perp[a_d,Z]\alpha_{\rm mf})^2R^2}{20\hbar B_e} - E_0 \end{bmatrix},$$

$$H_{11} = \begin{bmatrix} -K\left(\partial^2_R + \frac{\partial_R}{R} - \frac{(\ell-3)^2+1}{R^2}\right) + \frac{(f_\perp[a_d,Z]\alpha_{\rm mf})^2R^2}{10\hbar B_e} - E_1 & 2T\frac{\ell-3}{R^2} - \frac{\Delta_{\rm hf}}{2} \\ 2K\frac{\ell-3}{R^2} - \frac{\Delta_{\rm hf}}{2} & -K\left(\partial^2_R + \frac{\partial_R}{R} - \frac{(\ell-1)^2+1}{R^2}\right) - \frac{(f_\perp[a_d,Z]\alpha_{\rm mf})R^2}{20\hbar B_e} - E_1 \end{bmatrix}, \tag{14}$$

$$H_{01} = -\frac{3\delta(f_\perp[a_d,Z]\alpha_{\rm mf})^2R^2}{40\hbar B_e}\begin{bmatrix} 0 & 1 \\ 1 & 0 \end{bmatrix},$$

and $H_{10} = H_{01}$, where we have introduced the unit for kinetic energy $K = \frac{\hbar^2}{2m_{\rm mol}r_d^2}$ and neglected terms with strength $\propto \delta^2$. To solve Eqs. (13) and (14), as a first approximation we neglect the off-diagonal elements H_{01}, H_{10}, and $\Delta_{\rm hf}$, since $\delta \ll 1$. Later on in Sec. VI, we consider the consequence of H_{01}, H_{10}, and $\Delta_{\rm hf} \neq 0$ on the trap lifetime. Within this approximation, the Schrödinger

equation becomes

$$\begin{bmatrix} -K\left(\partial_R^2+\frac{\partial_R}{R}-\frac{(\ell-1)^2+1}{R^2}\right)+\frac{(f_\perp[a_d,Z]\alpha_{\rm mf})^2R^2}{10\hbar B_e}-E_j & 2K\frac{\ell-1}{R^2} \\ 2K\frac{\ell-1}{R^2} & -K\left(\partial_R^2+\frac{\partial_R}{R}-\frac{(\ell-1)^2+1}{R^2}\right)-\frac{(f_\perp[a_d,Z]\alpha_{\rm mf})^2R^2}{20\hbar B_e}-E_j \end{bmatrix}=\epsilon\begin{bmatrix} t_\ell^j[R] \\ u_\ell^j[R] \end{bmatrix}, \quad (15)$$

Note that the nanorod-dependent potential term (that depends on $f_\perp$) describes a harmonic trap for the upper part of Eq. (15), while it comes with the opposite sign in the lower block. Consequently, we divide Eq. (15) in two parts, the diagonal part where $t_\ell^j[R]$ denotes bound (trapped) states due to the R^2 potential and $u_\ell^j[R]$ denotes untrapped states with positive energy ($\epsilon>0$). A coupling between the two is given by the off-diagonal term. We notice in Eq. (15) that apart from the diagonal energy shift E_j, the equation of motion is independent of the hyperfine internal index j. For $\ell=1$, the off-diagonal part vanishes. Neglecting it at first for all ℓ, the differential equation for $t_\ell^j[R]\equiv t_\ell[R]$ can be transformed to associated Laguerre equations with known solutions. The eigenvectors and eigenenergies are given by

$$\begin{aligned} |t^j;\ell;N;\mathcal{N}=1\rangle &= e^{i(\ell-1)\varphi}\,|t,\ell N\rangle\,|-,\varphi\rangle\,, \\ \langle\vec{\tilde{R}}\mid t,\ell N\rangle &= \frac{\sqrt{2}(\tilde{R})^{\ell_{\rm eff}}\exp[-\tilde{R}^2/2]\mathcal{L}_N^{\ell_{\rm eff}}[\tilde{R}^2]}{(\Gamma[N+\ell_{\rm eff}+1]/N!)^{1/2}}, \quad (16) \\ \epsilon_{\ell,N}[a_d,Z] &= (2N+\ell_{\rm eff}+1)\hbar\omega[a_d,Z], \end{aligned}$$

where

$$\tilde{R}=R/\sigma[a_d,Z], \quad (17)$$

$$\ell_{\rm eff}=\sqrt{(\ell-1)^2+1}, \quad (18)$$

and $\Gamma[\cdots]$ is the Γ function. The quantum number of the radial motion of the trapped molecules is represented by non-negative integers N, with $N=0$ representing the lowest energy state. The Z-dependent oscillator width ($\sigma[a_d,Z]$) and frequency $\omega[a_d,Z]$ have the form

$$\begin{aligned} \sigma^2[a_d,Z]\equiv(\sigma[Z])^2 &= \frac{(10K\hbar B_e)^{1/2}}{f_\perp[a_d,Z]\alpha_{\rm mf}}, \\ \hbar\omega[a_d,Z] &= |\alpha_{\rm mf}|\,f_\perp[a_d,Z]\left(\frac{2K}{5\hbar B_e}\right)^{1/2}. \quad (19) \end{aligned}$$

From Eq. (16) it is clear that $\ell=1$ is lowest in energy and is nondegenerate. All other levels are twofold degenerate between the pair of states, $|t^j;-\ell+2;N;\mathcal{N}=1\rangle\,,|t^j;\ell;N;\mathcal{N}=1\rangle\,,\ell>1$. Looking into the radial distribution of the trapped states in Eq. (16), we see that the wave function vanishes at $R=0$. As a result, the effect of the cross term in Eq. (15) will be small. Moreover, for $N=0$, the excitation energy from the lowest energy state is given by $\delta\epsilon=\epsilon_{0,0}[a_d,Z]-\epsilon_{1,0}[a_d,Z]=\epsilon_{2,0}[a_d,Z]-\epsilon_{1,0}[a_d,Z]=(\sqrt{2}-1)\hbar\omega[a_d,Z]$. Next, we discuss the properties of the trap. It is clear that as the molecule is held closer to the surface, the trapping frequency increases as noted in Fig. 6(a). For such states to be trapped along Z, one needs an external force to keep the molecule near the nanostructure; this matter will be addressed in the next section. Additionally, by increasing the lattice constant a_d up to a certain value, one can also increase the trap frequency.

To qualitatively characterize the number of trapped states present, first we define the effective potential without the quadratic approximation as $V_{\rm trap}[\vec{\rho}]=\frac{|E_-[\vec{\rho}]|^2\alpha_{\rm mf}^2}{10\hbar B_e}$. As seen from Fig. 2(a), the trap height is minimal along $\varphi=0$ or $\pi/2$, and consequently the trap depth is defined as

$$V_{\rm depth}[a_d,Z]=V_{\rm trap}[R=a_d/2,\varphi=0,Z]. \quad (20)$$

Then the quantity $N_{\rm max}=V_{\rm depth}[a_d,Z]/2\hbar\omega[a_d,Z]$ gives an estimate for the number of trapped states; it is plotted in Fig. 6(b). We see that as the lattice constant decreases, the trap becomes shallow. For a fixed lattice constant, as expected, bringing the molecule closer to the surface results in an increased number of trapped states. Approximately, the trap ceases to exist as Z increases and $\hbar\omega[a_d,Z]\approx V_{\rm depth}[a_d,Z]$ is reached. For the parameters given in Tables I and II, and using Eq. (19), we find that for $a_d=2.25$ and at $Z=16$ the trapping frequency is $\omega[2.25,16]\approx 0.5$ MHz; cf. Fig. 6(a).

V. TRAPPING THE MOLECULES ALONG Z DIRECTION

In this section, we explain the mechanisms for providing trap for molecules along the Z direction.

A. Optical trapping mechanism

From the trapping energy, Eq. (16), it can be noticed that as the molecule in the (laterally) trapped state moves closer to the surface, the trap energy increases. Hence, the molecules will be pushed away from the surface. To prevent such an escape, we locally trap the molecules along the Z direction by employing a standing-wave optical laser field far red-detuned from the excited electronic states. Via the AC Stark effect, this attracts the molecule to the high-intensity region of the beam. However, the presence of such a field can lead to loss of molecules as components of the laser field polarized in the XY plane will strongly mix the trapped and untrapped internal states [33] described above. To prevent such polarization loss, we propose

TABLE I. Ferroelectric parameters for 0D and 1D traps.

	P (C m^{-2})	r_d (nm)	$a_{\rm latt}$ (nm)	h_d (nm)	$\frac{\alpha_{\rm mf}}{\hbar B_e}$	$\frac{K}{\hbar B_e}$
0D	10^{-1}	60	∞	180	5.8×10^3	1.2×10^{-5}
1D	2.5×10^{-1}	45	200	135	2.9×10^4	2.2×10^{-5}

TABLE II. Molecular parameters for RbCs

μ (Debye)	$m_{\rm mol}$ (10^{-26}kg)	B_e (GHz)
1.22	37	0.5

to use light beams propagating along the $\pm Z$ direction with a focused waist along the Y direction and a longitudinal field component along the Z direction. Moreover, the longitudinal field component needs to be much stronger than the transverse field component in the trapping region. Furthermore, we keep in mind that we want to generalize our trapping geometry from 0D to 1D, which means that the property of the beam should be approximately unaltered by translation along either the X or Y axis. To realize such a beam, we pass a Hermite-Gaussian wave through a cylindrical lens to focus at $Z = Z_0$ along the Y axis. As a zeroth-order approximation [34] ($a_d/\lambda \ll 1$, where λ is the laser wavelength), we neglect the effect of the nanostructure on the laser field at the molecular position so long as $\lambda/a_d > n$, where n is the refractive index of the ferroelectric substrate. This condition is equivalent to the physical situation that only the zeroth-order diffraction mode exists and the coupling to the guided modes of the periodic dielectric system is minimal due to normal incidence. For the incident field, we assume $\mathcal{E}^{\pm}_{\rm inc} = \sqrt{P_{in}}(0,2Y/w_0,0)\exp[-Y^2/w_0^2 \pm ikZ - i\Omega_{\rm las}t]$, where $P_{\rm in}$ denotes the laser power, w_0 is the beam waist, and $k = 2\pi/\lambda$. Such a mode can be created by passing a Gaussian wave through a π-phase plate [35]. Along the X direction, we have assumed a uniform field distribution. The time-independent contribution of the light field after focusing through a cylindrical lens (cylinder axis along $\hat{X}$) is given by $\mathcal{E}^{\pm}_{\rm las} = (0,\mathcal{E}^{\pm}_Y,\mathcal{E}^{\pm}_Z)$ (apart from a position-independent phase factor) [35,36],

$$\begin{aligned}\mathcal{E}^{\pm}_Y[Y,Z] &= \sqrt{P_{\rm in}}\frac{2kf^2}{w_0}\int_{\psi_1}^{-\psi_1} F[\psi]\cos^{3/2}[\psi]\sin[\psi] \\ &\quad\times \exp[\pm ikY\sin[\psi] \pm ik(Z \mp Z_0)\cos[\psi]]d\psi, \\ \mathcal{E}^{\pm}_Z[Y,Z] &= \sqrt{P_{\rm in}}\frac{2kf^2}{w_0}\int_{\psi_1}^{-\psi_1} F[\psi]\cos^{1/2}[\psi]\sin^2[\psi] \\ &\quad\times \exp[\pm ikY\sin[\psi] \pm ik(Z \mp Z_0)\cos[\psi]]d\psi,\end{aligned} \tag{21}$$

where $F[\psi] = \exp[-f^2\sin[\psi]^2/w_0^2]$ is the window function of the lens and f is its focal length. The numerical aperture of the lens is given by $\sin[\psi_1] = a_0/f$, where a_0 is the width of the pupil. The total laser field is given by adding two counterpropagating fields in Eq. (21) and defined as $\mathcal{E}_{\rm tot}[Y,Z] = (0,\mathcal{E}^Y_{\rm tot}[Y,Z],\mathcal{E}^Z_{\rm tot}[Y,Z])$. The total Z field shows a maximum at the focal line $Z = Z_0$, $Y = 0$ as seen in Fig. 4(a). From Eq. (21), it is clear that at $Y = 0$, $\mathcal{E}^{\pm}_Y[Y,Z] = 0$ as the integrand is odd under $\psi \to -\psi$. From Fig. 4(b), we see that at the line $Z = Z_0, Y = 0$, the Y component of the total field vanishes. This is due to the out-of-phase oscillation of the Y field as a function of Z. As a result, for $Z \approx Z_0, Y \to 0$, we are always in a region where the longitudinal Z component is much stronger than the transverse component and for $Z \to Z_0, Y = 0$, the laser intensity is approximately quadratic: $|\mathcal{E}^Z_{\rm tot}[0,Z]|^2 \approx I_0(1-\beta(Z-Z_0)^2/\lambda^2), \mathcal{E}^Y_{\rm tot} = 0$, where $\beta \approx 4\pi^2$ is a constant denoting curvature of the intensity profile near $Z = Z_0$ and I_0 is the total intensity of the lasers after focusing.

Next, we consider the effective laser-induced potential for $\mathcal{N} = 1$ molecules. The laser-molecule interaction Hamiltonian projected onto the $\mathcal{M}_{\mathcal{N}=1} \in \{0,\pm1\}$ subspace is given by (apart from a constant shift in energy $= -\alpha_1 I_0$) [33,37,38] by

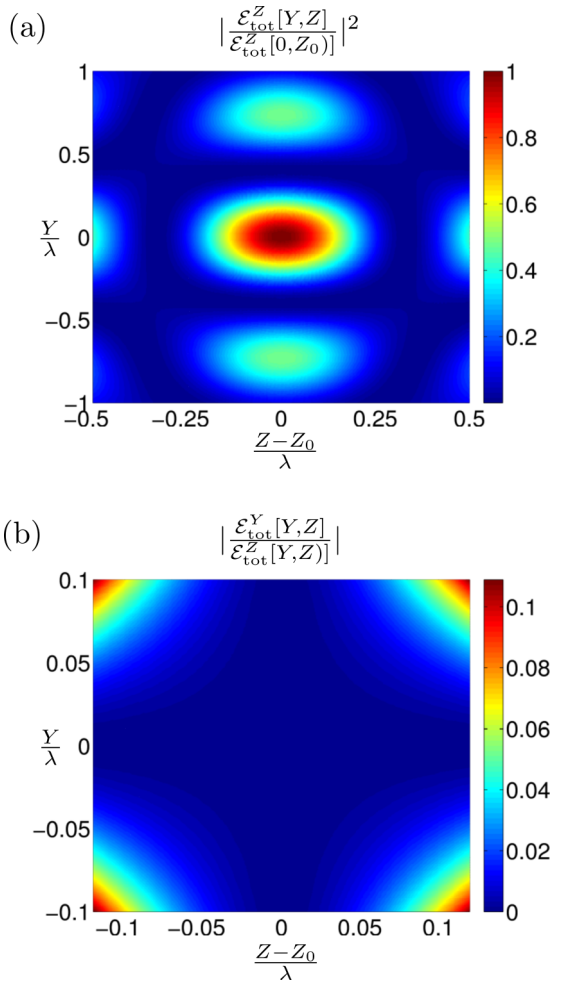

FIG. 4. (a) Plot of the longitudinal Z component of the total electric field. (b) Ratio between the transverse Y component and the longitudinal Z component is shown. The limits on the axis are different in panels (a) and (b). The parameters are, $\psi_1 = \pi/3$, $f/w_0 = 1.15$.

$$\begin{aligned}\frac{V^1_{\rm light}}{I_0} &= -\alpha_0\sum_{\mathcal{I}_{\rm col}}|1,0,\mathcal{I}_{\rm col}\rangle\langle 1,0,\mathcal{I}_{\rm col}| \\ &\quad+\alpha_1 V_Z\sum_{\substack{\mathcal{M}_1=\pm1\\ \mathcal{I}_{\rm col}}}|1,\mathcal{M}_1,\mathcal{I}_{\rm col}\rangle\langle 1,\mathcal{M}_1,\mathcal{I}_{\rm col}|,\end{aligned} \tag{22}$$

where $V_Z = \sin^2[\frac{2\pi(Z-Z_0)}{\lambda}]$, and α_1 is the polarizability of the $|\pm1\rangle$ states for a Z-polarized light field, which can be expressed as $\alpha_1 = (\alpha_\parallel + 4\alpha_\perp)/5$, where $\alpha_\parallel, \alpha_\perp$ are anisotropic polarizabilities of the molecule. Similarly, $\alpha_0 = 2(\alpha_\parallel - \alpha_\perp)/5$, which shows that the $\mathcal{M}_1 = 0$ state will be detuned in energy from the $\mathcal{M}_1 = \pm1$ states. Moreover, we consider laser strengths such that the detuning $\alpha_0 I_0$ is much larger than the transverse trap frequency $\hbar\omega[a_d,Z]$. For a laser strength of $I_0 \sim 0.1$ MW cm^{-2} and the trap frequency range considered in the present paper, typically, $\alpha_0 I_0/(\hbar\omega[a_d,Z]) \sim 20$ will exponentially suppress the loss rate to the $\mathcal{M}_1 = 0$ state by an approximate factor $e^{-\alpha_0 I_0/(\hbar\omega[a_d,Z])}$. The exponential factor arises due to the overlap integral between the trapped and the

continuum state with energy $\sim\alpha_0 I_0$. Then, combining Eqs. (16) and (22), the total effective potential along the Z direction seen by the trapped state is given by

$$V^1_{\rm eff}[Z] = \epsilon_{\ell,N}[Z] + \alpha_1 I_0 \sin^2\left[\frac{2\pi(Z-Z_0)}{\lambda}\right],$$
$$\approx V^1_{\rm eff}[Z_1] + \left.\frac{d^2 V^1_{\rm eff}[Z]}{2dZ^2}\right|_{Z=Z_1}(Z-Z_1)^2, \qquad (23)$$

where in the second line we have Taylor expanded the potential around the local minimum Z_1 (the subscript 1 is to keep track of the rotational level). We find that for the region of Z with minimized loss rate (discussed in the next section) the local minimum of Eq. (23) coincides with $Z_1 \approx Z_0$ for a laser with wavelength $\lambda = 1090$ nm with focal plane $Z_0 \sim 16$ and $I_0 \sim 0.1$ MW cm^{-2}. The approximate ground state along the Z direction is expressed as

$$\Phi_Z = \left(\frac{1}{\pi\sigma_Z{}^2}\right)^{1/4} \exp\left[-\frac{(Z-Z_0)^2}{2\sigma_Z{}^2}\right],$$

where the wave-function width is given by $\sigma_Z{}^2 = \left(\frac{d^2 V^1_{\rm eff}[Z]}{2dZ^2}|_{Z=Z_0}\right)^{-1/2}$. For the parameters considered here, $\alpha_1 I_0 (r_d/\lambda)^2 \gg \omega[a_d, Z]$ and as a result the trap frequency in the Z direction is given by $\omega_Z = 4\pi\sqrt{\alpha_1 I_0 K}(r_d/\lambda)$.

1. Laser-induced loss

Because of the red-detuned nature of the laser light, we trap the molecule at an intensity maximum. This can lead to molecular loss due to the imaginary part of the polarizability [37]. For a laser wavelength of 1 μm, the imaginary part is 10^{-7}–10^{-8} times weaker than the real part. Thus a laser intensity of $I_0 \sim 0.1$ MW cm^{-2} gives a lifetime in the order of 1–10 s. One way to further increase the lifetime is by increasing the laser wavelength to around 1.5 μm, where one is off-resonant from all excited states and as a result the imaginary part should decrease exponentially with respect to frequency shift: As seen in Ref. [37], the real part of the polarizability remains the same, but the imaginary part decreases by an order of magnitude or more. As a result, one can increase the molecular lifetime to tens of seconds although the trapping along Z direction becomes shallow.

B. Electrostatic trapping along Z axis

As an alternative to optical trapping along the Z direction, we also sketch a purely electrostatic proposal involving two 0D structures, as shown in Fig. 5(a). The distance between the two structures is given by L_Z. Following Eq. (10), the total azimuthal electric field $E_-[\vec{\rho}]$ then can be written as $E_-[\vec{\rho}] \approx i f_\perp[a_d, Z]{\rm Re}^{i\varphi}$. In Fig. 5(b), we plot $f_\perp[a_d, Z]$ for $a_d = 2.25$ and $L_Z = 32$. We clearly see that along Z direction, the potential increases from the center of the trap $Z_0 = L_Z/2$. From using the parameters in Table I, we find that the corresponding trap has the following parameters: $\omega[2.25, Z] \approx 0.5 \times 10^{-4} B_e, \omega_Z \approx .5 \times 10^{-5} B_e$, where ω_Z is the frequency along the Z direction.

Though the optical trapping maybe preferable for loading from ultracold samples, the electrostatic method is preferable for molecules for which optical preparation is not available.

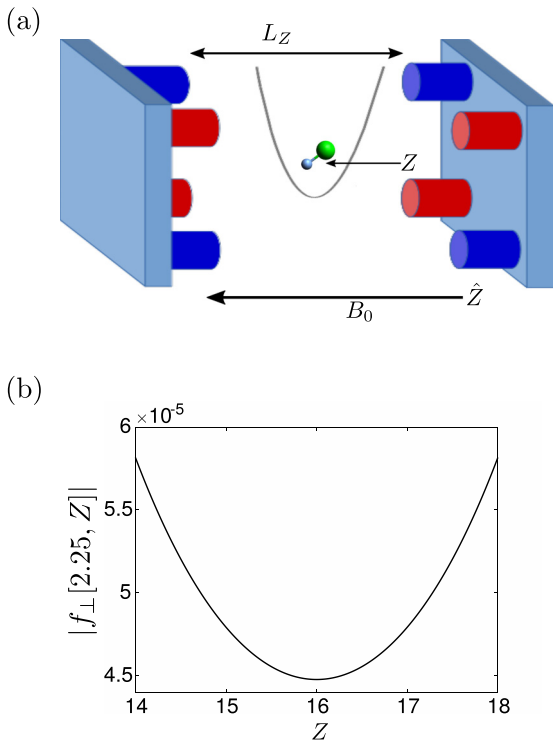

FIG. 5. Electrostatic 0D trap: (a) Two 0D structures facing each other and the corresponding Z axis. Nanorods of similar polarization in both nanostructure is aligned with each other. (b) We show the effective shape of the electric-field fitting function.

Moreover, it can be readily extended to 2D array structure as unlike the optical trapping, we are not constrained by special polarization properties of the laser. A detailed analysis of such 2D array is beyond the scope of the present paper.

VI. MOLECULE LOSS RATES DUE TO NONADIABATIC AND HYPERFINE COUPLING

Next, we discuss various couplings that can transfer trapped states to untrapped states. The first approximation arises as a nonadiabatic effect to the Hamiltonian due to the position dependence of the perturbation in Eq. (8). As discussed in Appendix B, in the present case, such corrections are found to be negligible.

In the remaining part of this section, we describe important loss mechanisms.

A. Loss due to intrastate coupling

The next correction arises due to the nonzero off-diagonal elements of H_{11} in Eq. (15). These elements couple the trapped state $|t^j;\ell;N;\mathcal{N}=1\rangle$ to the continuum states $|u^j;\ell;\mathcal{N}=1\rangle$ with same angular momentum ℓ as described by the off-diagonal terms in Eq. (15). It is readily seen that a special situation arises for $\ell = 1$ as the off-diagonal term vanishes and there is no coupling to the untrapped state. This exact decoupling of trapped and untrapped states no longer holds for $\ell \neq 1$. To qualitatively describe the effect of the untrapped states, we invoke Fermi's golden rule by considering resonant coupling of the trapped state $|t^j;\ell;N;\mathcal{N}=1\rangle$ to the continuum states

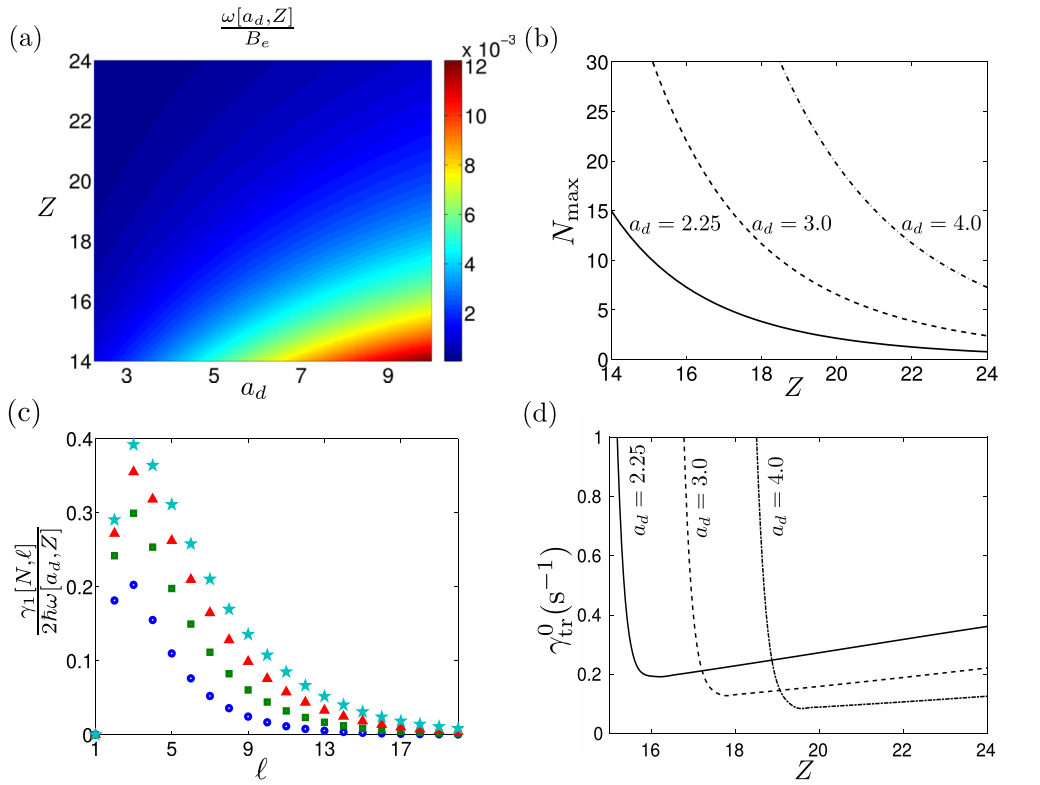

FIG. 6. (a) The trap frequency is shown as a function of Z and a_d for the parameters listed in Tables I and II. (b) Relative trap depth $N_{\max}$ is shown as a function of Z for $a_d = 2.25$ (solid line), 3.0 (dashed line), and 4.0 (dash-dotted line). (c) The decay rate $\gamma_1[\ell,N]$ from Eq. (24) is plotted as a function of ℓ for $N = 0(\circ),1(\square),2(\triangle),3(\star)$. (d) Total nonadiabatic and hyperfine-induced loss rate $\gamma_{\rm tr}^0$ is plotted as a function of Z for $a_d = 2.25$ (solid line), 3.0 (dashed line), and 4.0 (dash-dotted line). The parameters are shown in Tables I and II.

with energy $\epsilon_{\ell,N} > 0$ via the off-diagonal term in Eq. (15). The solution for the untrapped state then becomes $\langle \vec{\tilde{R}} \mid u,\ell M\rangle = \sqrt{2}\mathcal{J}_{\ell_{\rm eff}}[\alpha_{\ell,M}\tilde{R}/\tilde{R}_0]/(\tilde{R}_0|\mathcal{J}_{\ell_{\rm eff}+1}[\alpha_{\ell,M}]|)$, where $\mathcal{J}_\ell[]$ denotes the Bessel function of order ℓ. We use a cylindrical hard-wall boundary condition with radius $\tilde{R}_0 \to \infty$ and $\alpha_{\ell,M}$ is Mth zero of the Bessel function, $\mathcal{J}_{\ell_{\rm eff}}[x\alpha_{\ell,M}] = 0$. The resonant energy condition is given by $\alpha^2_{\ell,M_{\rm res}}/\tilde{R}_0^2 = 2(2N + \ell_{\rm eff} + 1) + \tilde{R}^2/2$. The decay rates for the trapped state $|t^j;\ell;N;\mathcal{N} = 1\rangle$ reads

$$\frac{\gamma_1[\ell,N]}{\hbar\omega[a_d,Z]} = 2\pi\mathcal{D}\big[\alpha_{\ell,M_{\rm res}}\big]|\,\langle t,\ell N \mid \tilde{R}^{-2} \mid u,\ell M_{\rm res}\rangle\,|^2, \quad (24)$$

where the density of states in dimensionless units is $\mathcal{D}[\alpha_{\ell,M}] = \tilde{R}_0^2/(2\pi\alpha_{\ell,M})$. The use of Fermi's golden rule remains valid as long as the decay rates are lower than the minimum energy gap, $|\epsilon_{\ell,N+1} - \epsilon_{\ell,N}| = 2\hbar\omega[a_d,Z] > \gamma_1[\ell,N]$, which is fulfilled for all ℓ. We plot the decay rate in Fig. 6(c) for various ℓ,N. Because of the symmetry around $\ell = 1$, $\gamma[-\ell,N] = \gamma[\ell+2,N]$ for $\ell \geqslant 0$. We find that the decay rate is maximal for $\ell = 5,-3$ and then decreases for larger ℓ. Note that as the effective potentials are always of finite height, as a result the decay rates are valid as long as $\epsilon_{\ell,N} \lesssim V_{\rm deptth}$. We point out that trapped states with this kind of long lifetime ($|t;\ell = 1;N;\mathcal{N} = 1\rangle$) do not exist for traps using the linear Stark shift (e.g., for asymmetric-top molecules). As a result, for those traps, one needs a larger trap size (which decreases K) to suppress molecule loss. The reason behind this is that there exists no angular momentum channel for which the coupling to untrapped states vanishes.

B. Loss due to hyperfine-structure-induced coupling

Hyperfine-induced coupling has two contributions. The first one induces intrastate transitions due to the presence of $\Delta_{\rm hf}$ in H_{00} and H_{11} in Eq. (14). From Table III and Fig. 6(a), we find that the trap frequency is much larger than the detuning ($\Delta_{\rm hf}/\omega[a_d,Z] \approx 0$) and as a result we neglect its effect. The next correction arises due to the matrix elements of H_{01},H_{10} in Eq. (14) which are of order $\delta \ll 1$ (cf. Table III) and induce coupling between different internal states denoted by j. As the off-diagonal elements of H_{01},H_{10} are nonzero, these elements can couple a trapped state to continuum states belonging to a different hyperfine structure. On the hand, there is a detuning due to the presence of a magnetic field with magnitude $|E_0 - E_1|$. As a result, for a sufficiently strong magnetic field, the transition is suppressed for $|E_0 - E_1|/\omega[a_d,Z] \gg 1$. Such a

TABLE III. Parameters representing molecular states in Eqs. (2) and (3) and the corresponding magnetic field and energy scales.

	B_0 (T)	δ	δ_1	$\frac{E_1-E_0}{\hbar B_e}$	$\frac{\Delta_{\rm hf}}{1\hbar B_e}$
0D	0.1	0.054	0.058	5.5×10^{-3}	0.0
1D	2.0	0.003	0.003	5.5×10^{-1}	3.7×10^{-4}

suppression occurs as the trapped $|t^0,10\rangle$ state is confined deep inside the classically forbidden region of the continuum states $|u^1,-1\rangle$.

Though for magnetic fields available in a laboratory, one cannot reach a regime of complete suppression. As a result, we calculate the transition rate from the trapped state (for details, see Appendix C), which we denote by $\gamma_{\rm hf}^j$. Their definitions are given in Eqs. (C2) and (C3). The most important thing to notice by dimensional analysis of H_{01}, H_{10} is that $\gamma_{\rm hf}^j \propto \delta^2\omega[a_d,Z]$.

C. Loss rate due to the R^3 dependence of electric field

Additional loss channels are also present due to the second term $\propto R^3\exp[-3i\varphi]$ in Eq. (10) which modifies the $E_\pm$ electric field components. As a result, the effective potential in Eq. (11) will be modified with an additional term $\propto R^4$. As shown in Appendix D, the correction leads to coupling within the same hyperfine manifold j between states belonging to different ℓ quantum number. The modified decay rate due to coupling of $\ell=1, N=0$ motional state to other lossy trapped state is given by (for details, see Appendix D)

$$\gamma_t = \left(\frac{f_{-3\perp}[a_d,Z]K}{f_\perp[a_d,Z]\hbar\omega[a_d,Z]}\right)^2 \sum_{\ell'=-3,5}\sum_{N'} \times \left|\frac{V_{1,0;\ell',N'}}{-2N'+1-\sqrt{(\ell'-1)^2+1}}\right|^2 \gamma_1[\ell',N']. \quad (25)$$

We like to point out that the use of perturbation theory may become invalid for calculating the decay for states with higher ℓ due to the presence of nearby degenerate states. In that case, one can get the decay rates by concentrating on the degenerate subspace. If that is not the case, we find that the sum in Eq. (25) approximately converges for $|N'|<2$. As a result, for a consistent decay rate from $N=0$ state, one needs to have a trap with $N_{\rm max}\sim 2$. Otherwise, one also need to consider the continuum states due to the finite hight of the trapped potential.

The next source of loss originates from coupling of the $\ell=1$ state to continuum states with different ℓ quantum number as shown in Appendix D. The loss rate for the $N=0,\ell=1$ state consequently is given by

$$\gamma_{\rm c} = 2\pi\left(\frac{3f_{-3}[a_d,Z]}{4f_\perp[a_d,Z]\hbar\omega[a_d,Z]}\right)^2 \frac{K^2\mathcal{D}\left[\alpha_{\ell,M_{\rm res}}\right]}{\hbar\omega[a_d,Z]} \times \sum_{\ell=-3,5} |\langle t,\ell N \mid \tilde{R}^4 \mid u,\ell M_{\rm res}\rangle|^2, \quad (26)$$

with the resonant energy condition $\alpha^2_{\ell,M_{\rm res}}/\tilde{R}_0^2 = 2(\ell_{\rm eff}+1)+\tilde{R}^2/2$. To find the lifetime, we assume the parameters as in Tables I and II and the unperturbed loss rate from Eq. (24).

D. Total trapped molecule loss rate

To find the total loss rate, we notice from Eqs. (26) and (25) and Sec. VI B that the hyperfine-induced rate of level j scales as $\gamma_{\rm hf}^j \propto \omega[a_d,Z]$. On the other hand, from Eqs. (25), (26), and (24), we find that higher order correction to the electric field gives rise to loss rates $\gamma_{t,c}\propto\omega^{-1}[a_d,Z]$. As a result, once we fix the ferroelectric polarization and the nanorod dimensions, by changing the position of the molecule along Z, one can find an optimum solution. To this end, we define the total molecule loss rate by adding Eqs. (25) and (26) and hyperfine-induced loss rate,

$$\gamma_{\rm tr}^j = \gamma_{\rm hf}^j + \gamma_t + \gamma_c, \quad (27)$$

which is pictorially shown in Fig. 6(d). From Figs. 6(b) and 6(d), we find that for $a_d=2.25$ ($a_d=135$ nm for parameters in Table I) and with $N_{\rm max}\approx 10$, the loss rate is minimized around a distance $Z\approx 16.0$ ($\approx 0.96\,\mu$m) with decay rate $\gamma_{\rm tr}^0\approx 0.2$ Hz (lifetime of $\sim$5 s). By increasing the distance between the nanorods, one sees that the lifetime is increased up to $\sim$10 s for $a_d=4.0$. Another way to increase the lifetime is by increasing the magnetic field which will increase $|E_1-E_0|$ between the hyperfine states $j=0,1$ and decreasing the hyperfine loss rates in Sec. VI B. In Appendix E, we show the effect of increased magnetic field with increased lifetime of $\sim$20 s for $Z=14$.

We find that the remaining nonadiabatic loss channels due to the E_Z field in Eq. (8) give a much longer lifetime and as a result they are discussed in Appendixes F and G.

VII. LOSS DUE TO SURFACE PROXIMITY

The present section considers the loss of trapped molecules due to thermalization in the presence of the substrate surface. Such losses exist irrespective of the presence or absence of a trapping potential. The loss rates arise from two primary sources: (i) photon fluctuations of the vacuum-substrate interface and (ii) phonon fluctuations in the surface of the substrate.

A. Radiative loss

A source of loss of molecules is the coupling of rotational levels to the black-body radiation modified by nanorods and surface of the 2D substrate. The coupling frequency then corresponds to a rotational transition which for $^1\Sigma$ molecules generally lies in the GHz region and subsequently we neglect the hyperfine splitting. The coupling wavelength corresponds to $\lambda_{\rm rot}\sim 10^{-1}$m. The height of the nanorods is negligible compared to the coupling wavelength, $h/\lambda_{\rm rot}\ll 1$. As a result, from the viewpoint of effective medium theory, the Fresnel reflection coefficients only get modified by a negligible amount, $\propto h/\lambda_{\rm rot}$ [39], and we can neglect the effect of the periodic nanorods. Moreover, the lifetime of the molecule is dominated by the surface and, as a result, we neglect the free-space contribution. Assuming that the substrate- and free-space photons are in equilibrium with temperature $k_bT\gg\hbar B_e$, and following Refs. [40,41], the rotational heating rate for a molecule from the $|\mathcal{N}=1,\mathcal{M}_\mathcal{N}=\pm1\rangle$ state is given by

$$\gamma_h = \gamma_0 + \frac{\mu^2}{8\pi\epsilon_0 Z_{\rm mol-sub}^3}\frac{k_BT}{2\hbar B_e}\frac{Qf}{2B_e}\frac{{\rm Re}[\epsilon_s]}{({\rm Re}[\epsilon_s]+1)^2} \times\left(\langle D_{00}^-\rangle^2 + \frac{\langle D_{22}^+\rangle^2}{2^2} + \frac{\langle D_{20}^-\rangle^2}{2^2} + \frac{\langle D_{21}^Z\rangle^2}{2}\right), \quad (28)$$

where γ_0 is the free-space heating rate, $Z_{\rm mol-sub}$ is the distance of the molecule from the substrate, ϵ_s is the dielectric constant of the substrate, and the D_{ij} are dipole matrix elements

$$\langle D_{00}^-\rangle = \langle\mathcal{N}=0,\mathcal{M}_\mathcal{N}=0|\,\boldsymbol{T}^1_{-1}\,|\mathcal{N}=1,\mathcal{M}_\mathcal{N}=1\rangle,$$
$$\langle D_{22}^+\rangle = \langle\mathcal{N}=2,\mathcal{M}_\mathcal{N}=2|\,\boldsymbol{T}^1_{1}\,|\mathcal{N}=1,\mathcal{M}_\mathcal{N}=1\rangle,$$

$$\langle D_{20}^{-}\rangle = \langle \mathcal{N}=2,\mathcal{M}_{\mathcal{N}}=0|\, \boldsymbol{T}^{\mathbf{1}}_{-\mathbf{1}}\, |\mathcal{N}=1,\mathcal{M}_{\mathcal{N}}=1\rangle\,,$$
$$\langle D_{21}^{Z}\rangle = \langle \mathcal{N}=2,\mathcal{M}_{\mathcal{N}}=1|\, \boldsymbol{T}^{\mathbf{1}}_{\mathbf{0}}\, |\mathcal{N}=1,\mathcal{M}_{\mathcal{N}}=1\rangle\,.$$

Hence, the total heating rate is given given by the sum of the free-space and substrate-induced heating rates [40]. The lifetime of a RbCs molecule at 4K is on the order of $\sim 10^8$ s [40], and as a result we can practically neglect the free-space heating rate compared to the substrate-induced rate. To estimate the latter, we use fused quartz as an example whose dielectric properties are given by [42] $\mathrm{Re}[\epsilon_s] \approx 3.83$ and $Qf \approx 10^5$ GHz. The molecular heating rate then becomes $\gamma_{\mathrm{h}} \approx 0.02\ \mathrm{s}^{-1}$ at a distance of 1 μm (equivalent to $Z \approx 16$ in the unit of nanorod radius for the parameters in Table I) from the substrate for liquid helium temperature of 4K. The role of Casimir forces in such distance is negligible and is discussed qualitatively in Appendix H.

One possible way to extend the lifetime can be achieved by a 1D substrate with thickness d_{sub} near an integer multiple of $2\pi c_{\mathrm{light}}/(n_{\mathrm{sub}} B_e)$, where c_{light} is the speed of light and n_{sub} is the refractive index of the substrate. This reduces the reflection coefficient for light waves with perpendicular incidence (polarized in the XY plane). As a result, the important substrate effect comes from the electromagnetic waves with polarization along the Z direction, a change from the vacuum structure, which can increase the lifetime by a factor of 2. Another possible way to increase lifetime can be achieved be use of a glassy substrate with thickness $d_{\mathrm{sub}} \ll B_e^{-1}$, where B_e is given in cm^{-1}. In such cases, due to the long wavelength of the resonant light, the substrate will be invisible. Such a substrate can stand on thin pillars and as a result any macroscopic object will effectively be far away from the molecule.

B. Loss induced by vibrational modes of the substrate

The presence of long-wavelength vibrations in the 2D substrate also induces vibrations of the nanorods. This leads to an phonon-assisted coupling between the molecular rotational levels. As a result, there will be transitions between rotational levels leading to heating (similar to the radiative loss due to electromagnetic coupling). To gain a qualitative understanding, we model the surface of the substrate as a square lattice of atoms. Moreover, we also consider that the underlying arrangement of atoms in the nanorods are also cubic. For simplicity, we assume that atoms in both lattices have mass M and lattice constant a_S. We denote the equilibrium position of individual nanorod by $\vec{b}$. For long-wavelength phonons, vibrations of the atoms in the nanorods are all locked to the surface vibrations of the substrate. We first consider the effect of transverse acoustic phonon modes of the substrate surface. The displacement of the atoms are normal to the surface with magnitude $\boldsymbol{U}[\vec{b}]$. In the second quantized form, we write the displacement operator in momentum space [two-dimensional momentum $\vec{k} = (k_x, k_y)$] as

$$\boldsymbol{U}[\vec{b}] = \sum_{\vec{k}} \boldsymbol{U}_{\vec{k}} e^{i\vec{k}\cdot\vec{b}},$$
$$\boldsymbol{U}_{\vec{k}} = \sqrt{\frac{\hbar}{2M\omega_{\vec{k}} r_d^2}}(\boldsymbol{a}_{\vec{k}} + \boldsymbol{a}^{\dagger}_{-\vec{k}}), \tag{29}$$

where the appearance of r_d is due to our choice of the unit of distance. The phonon creation and annihilation operators are denoted by $\boldsymbol{a}^{\dagger}_{\vec{k}}, \boldsymbol{a}_{\vec{k}}$ and the phonon dispersion relation is given in the long wavelength limit as $\omega_{\vec{k}} = ck$, where c is the sound velocity. In the limit where the molecules are far away from the nanorods, the electric field components due to the transverse displacement of a nanorod are expressed as $\boldsymbol{E}_{\eta} = \partial E_{\eta} \boldsymbol{U}[\vec{b}]$, where $\eta = \pm, Z$ and $\partial E_{\eta} = \frac{\partial E_{\eta}}{\partial Z}$ with the electric field given by Eq. (6), and as we are using the expression for only a single rod, $m_x = m_y = 0$ in this particular case. The total Hamiltonian is given by

$$\begin{aligned}
H_{\mathrm{tot}} &= H_{\mathrm{rot}} + H_{\mathrm{ph}} + H_{\mathrm{mol-ph}},\\
H_{\mathrm{rot}} &= \hbar B_e \sum_{\mathcal{N},\mathcal{M}_{\mathcal{N}}} \mathcal{N}(\mathcal{N}+1)\, |\mathcal{N},\mathcal{M}_{\mathcal{N}}\rangle\, \langle \mathcal{N},\mathcal{M}_{\mathcal{N}}|\,,\\
H_{\mathrm{ph}} &= \sum_{\vec{k}} (\boldsymbol{n}_{\vec{k}} + 1/2)\hbar\omega_{\vec{k}},\\
H_{\mathrm{mol-ph}} &= \sum_{\vec{k}} \boldsymbol{U}_{\vec{k}} \sum_{\substack{\mathcal{N}',\mathcal{M}'_{\mathcal{N}}\\ \mathcal{N},\mathcal{M}_{\mathcal{N}}}} V_{\mathcal{N}',\mathcal{M}_{\mathcal{N}'};\mathcal{N},\mathcal{M}_{\mathcal{N}}}\, |\mathcal{N}',\mathcal{M}_{\mathcal{N}'}\rangle\, \langle \mathcal{N},\mathcal{M}_{\mathcal{N}}|\,,
\end{aligned} \tag{30}$$

where in order to write the molecule-phonon interaction, we have assumed that we are interested in the long-wavelength limit and the molecular matrix element $V_{\mathcal{N}',\mathcal{M}_{\mathcal{N}'};\mathcal{N},\mathcal{M}_{\mathcal{N}}} = \langle \mathcal{N},\mathcal{M}_{\mathcal{N}}|\, \partial E_Z \boldsymbol{T}^{\mathbf{1}}_{\mathbf{0}} + \partial E_{-} \boldsymbol{T}^{\mathbf{1}}_{\mathbf{1}} + \partial E_{+} \boldsymbol{T}^{\mathbf{1}}_{-\mathbf{1}}\, |\mathcal{N}',\mathcal{M}_{\mathcal{N}'}\rangle$. For our present paper, we are specifically interested in transition rates from the molecular states $|\mathcal{N}=1,\mathcal{M}_{\mathcal{N}}=\pm 1\rangle$ which will couple to the states $|\mathcal{N}=0,2,\mathcal{M}_{\mathcal{N}}=0\rangle\,, |\mathcal{N}=2,\mathcal{M}_{\mathcal{N}}=\pm 1,\pm 2\rangle$ via absorption or emission of phonons with energy corresponding to the energy difference between the molecular levels. Similar to the electromagnetic case in Ref. [43], we find for the transition rate from $|\mathcal{N}=1,\mathcal{M}_{\mathcal{N}}=+1\rangle$ to $|\mathcal{N},\mathcal{M}_{\mathcal{N}}\rangle$

$$\begin{aligned}
\gamma_{\mathrm{ph}}[\mathcal{N},\mathcal{M}_{\mathcal{N}}] = \sum_{\vec{k},\vec{k}'} \sum_{n^i_{\vec{k}}, n^f_{\vec{k}'}} \delta\big[&(\mathcal{N}^2+\mathcal{N}-2)\hbar B_e\\
&+ \big(n^f_{\vec{k}'} - n^i_{\vec{k}}\big)\hbar\omega_{\vec{k}}\big] P[n_{\vec{k}}]\, \big|\langle n^f_{\vec{k}'}|\, \langle \mathcal{N},\mathcal{M}_{\mathcal{N}}|\\
&\times H_{\mathrm{mol-ph}}\, |1,1\rangle\, \big|n^i_{\vec{k}'}\big\rangle\big|^2,
\end{aligned} \tag{31}$$

where $|n^{i,f}_{\vec{k}}\rangle$ are phonon Fock states and $|1,1\rangle = |\mathcal{N}=1,\mathcal{M}_{\mathcal{N}}=1\rangle$. The thermal distribution of the phonon number $n^i_{\vec{k}}$ is given by $P[n^i_{\vec{k}}] = \exp[-n^i_{\vec{k}}\hbar\omega_{\vec{k}}/(k_B T)]/(\sum_{m_{\vec{k}}=0}^{\infty} \exp[-m_{\vec{k}}\hbar\omega_{\vec{k}}/(k_B T)])$ with T being the temperature. The δ function in Eq. (31) represents the resonance condition.

For general $^1\Sigma$ molecules, the rotational energy gap is in the GHz range. For a substrate with sound velocity $c = 5 \times 10^3\,\mathrm{m\,s}^{-1}$, the corresponding phonon wavelength is on the order of $k^{-1} \sim 10^{-6}$m which is much larger than the lattice constant a_S. Using Eqs. (29)–(31), we calculate the transition rates

$$\gamma_{\mathrm{ph}}[0,0] = \frac{\hbar D[\omega_{\vec{k}}]|\partial E_{+}|^2}{3Mr_d^2\omega_{\vec{k}}} \sum_n (n+1)P[n], \quad \omega_{\vec{k}} = 2B_e,$$
$$\gamma_{\mathrm{ph}}[2,\eta] = f_{\eta}\frac{\hbar D[\omega_{\vec{k}}]|\partial E_{+}|^2}{Mr_d^2\omega_{\vec{k}}} \sum_n nP[n], \quad \omega_{\vec{k}} = 4B_e, \tag{32}$$

where $\eta = 0,1,2$, $f_0 = 1/15, f_1 = 1/5, f_2 = 2/5$, and $D[\omega_{\vec{k}}] = a_S^2\omega_{\vec{k}}/(\pi^2 c^2)$ is the density of states for the phonon. The total transition rate from the $|\mathcal{N}=1,\mathcal{M}_{\mathcal{N}}=1\rangle$ state is given by $\gamma_{\rm ph}^{\rm tot} = \gamma_{\rm ph}[0,0] + \gamma_{\rm ph}[2,0] + \gamma_{\rm ph}[2,2] + \gamma_{\rm ph}[2,1]$. For a quantitative estimate, we assume a sound velocity of $c = 5\times10^3 \mathrm{m\,s^{-1}}$ (similar to the one in a quartz crystal), temperature $T = 10\,\mathrm{K}$, an atom mass for the substrate $M = 5\times10^{-26}\mathrm{kg}$ (mass of silicon), and a typical lattice constant of $a_S \sim 0.5\,\mathrm{nm}$. We place a molecule at a distance $\sqrt{X^2+Y^2} \sim 1, Z \approx 16$, which is similar to the trapping distance in our scheme with $r_d = 60\,\mathrm{nm}$. Inserting the parameters in Eq. (32), for RbCs molecules, the transition rate becomes $\gamma_{\rm ph}^{\rm tot} \approx 0.01\ \mathrm{s^{-1}}$. To see the combined effect of the four nanorods for a trapped molecule near the center of a square cell, we find that the heating rates in Eqs. (32) are multiplied by a factor $|\sum_{j_x=\pm1/2,j_y=\pm1/2}(-1)^{j_x+j_y}\exp[-ia_d(k_xj_x+k_yj_y)]|^2$. This is due to the phase in phonon amplitude [Eq. (29)] and the alternating polarization of the rods. For long phonon wavelengths $k^{-1} \gg a_d$, this results in a destructive interference and as a result the transition rate is decreased by a factor $\sim(ka_d)^4 \sim 10^{-4}$. Hence, near the center of the square cell in Fig. 1, molecules are more stable than in the corners.

Phonons with energies in the range of the trapping frequency can further heat up the molecules by coupling the motional states. Following a similar procedure as above, we found that the motional heating rate is dominated by the vibrations along the surface of substrate. The heating rate is given by

$$\gamma_{\rm motion} \propto \omega^2[a_d,Z]\left(\frac{\hbar D[\omega_{\vec{k}}]}{M\sigma^2[a_d,Z]\omega_{\vec{k}}}\right)\frac{k_BT}{\hbar\omega_{\vec{k}}},$$
$$\omega_{\vec{k}} = \omega[a_d,Z],$$

where the trapping frequency and width are given in Eqs. (19). The ω^2 term on the right-hand side comes from the square of the overlap of motional states. The second factor (in parentheses) originates from the overlap between the resonant phonon states, whereas the last fraction gives the thermal phonon number at the resonant frequency. For a molecule trapped at $Z \sim 1\,\mu\mathrm{m}$ ($Z = 16$ in units of r_d) from top of the nanorod with radius $r_d = 60\,\mathrm{nm}$, from Eq. (19) we find that $\omega[2.25,16] \sim 0.5\,\mathrm{MHz}$. For a temperature of $T = 4\mathrm{K}$, this given a heating rate of $\gamma_{\rm motion} \lesssim 10^{-2}\ \mathrm{s^{-1}}$.

VIII. 1D NANOTRAPS FOR MOLECULES

Using our 0D nanorod arrangement as a building block, we extend to a 1D structure by repeating the primitive square cell with a lattice constant of $a_{\rm latt}$, as shown in Fig. 1(b). Additionally, the polarization arrangement in each square cell is $\pi/2$ out of phase with its neighbor. Each nanorod is centered at $\vec{F}_{q,\boldsymbol{m}} = a_{\rm latt}q\hat{X} + a_d(m_x\hat{X} + m_y\hat{Y})/2$,where $q \in [-N_f, -N_f+1, \ldots, -1, 0, 1, \ldots, N_f-1, N_f]$. The total number of cells is given by $2N_f+1$. The polarization of each rod is defined as, $P[\vec{R}] = (-1)^{q+(m_x+m_y)/2}P\hat{Z}$ when $0 < |\vec{R} - \vec{F}_{q,\boldsymbol{m}}| < r_d$, $-h < Z < 0$; otherwise, it is zero. Also, the 0D structure can be considered as a special case of 1D structure with $a_{\rm latt} = \infty$.

In the 1D structure, we define electric fields equivalent to Eqs. (6) by replacing $R_{\boldsymbol{m}} \to R_{q,\boldsymbol{m}}$ with $\vec{R}_{q,\boldsymbol{m}} = \vec{R} - \vec{F}_{q,\boldsymbol{m}}$ and $\phi_{\boldsymbol{m}} \to \phi_{q,\boldsymbol{m}}$ with $\tan\phi_{q,\boldsymbol{m}} = (Y - m_ya_d)/(X - qa_{\rm latt} - m_xa_d)$. Similar to Eq. (7), the total electric field is given by

$$E_\eta[\vec{\rho}] = \sum_{q=-N_f}^{N_f}\sum_{\boldsymbol{m}}(-1)^{q+\frac{m_x+m_y}{2}}E_\eta[q,\boldsymbol{m};\vec{\rho}]\ \ (\eta = Z,-). \tag{33}$$

To look for the properties of the electric field, we first notice that the long-range nature of the dipole potential from neighboring cells strongly affects the trapping potential and lowers it significantly. Moreover, the absence of rotational symmetry leads to additional loss terms. Each square cell is centered at $(q,0)a_{\rm latt}$ and is bounded by the lines $X = (qa_{\rm latt} \pm a_d/2), |Y| = a_d/2$ as shown in Fig. 1(b). The alternating orientation of the cells generate electric-field distributions with out-of-phase neighboring square cells. Inside each square cell, the trap potential close to the center depends quadratically on $|E_-|$, the same as in 0D. In Fig. 7(a), we plot the $|E_-|^2$ along the X axis for a fixed Z with $N_f = 10, a_{\rm latt} = 2a_d$. It is clear that there is a potential minimum at the center of each square cell whereas there is a shift in the position of the minima for the boundary square cells. Moreover, the trap height at the boundary is higher, which will result in a reduced escape rate of the molecules from the boundary traps.

For a quantitative study, we define a local polar coordinate at each cell q as $R_q^2 = (X - qa_{\rm latt})^2 + Y^2$ and $\varphi_q = \tan[\frac{Y}{X-qa_{\rm latt}}]$. Similar to the 0D trap, the 1D trap is symmetric under reflection at the X or Y axes (and change of polarization) and the Fourier coefficients of the azimuthal field E_- with even power vanishes. The rotational symmetry about center of the square is violated. However, as noted in Appendix I, the leading-order term in E_- is still $\propto iRe^{i\varphi}$. Thus we can write the electric field at the center of the cell as

$$E_{-q}[\vec{\rho}] \approx iR_q(F_\perp[a_d,a_{\rm latt},Z])\exp[i\varphi_q] + i\sum_{\eta=\pm3}F_\eta[a_d,a_{\rm latt},Z]R_q^3\exp[i\eta\varphi_q],$$
$$E_{Zq}[\vec{R}_q,Z] \approx F_z[a_d,a_{\rm latt},Z]R_q^2\sin[2\varphi_q], \tag{34}$$

where $R_q < a_d/2$. In contrast with the 0D case in Eq. (10), the electric field contains both of ±3 azimuthal components. The fitting functions are shown in Fig. 7(b) for parameters in Table I. Comparing it with the $0D$ case (Fig. 3), we see that for similar a_d, $|F_\perp[a_d,a_{\rm latt},Z]| < |f_\perp[a_d,Z]|$ and as a result yields much weaker potential. Only in the situation of $a_{\rm latt} \to \infty$ do they become equal as the 1D trap becomes equivalent to 0D trap. Otherwise, the magnitude of $|F_\perp[a_d,a_{\rm latt},Z]|$ can be boosted by trapping the molecules nearer to the nanorods and by increasing the total polarization of the nanorods. Moreover, for fitting functions to R^3 component (responsible for nonadiabatic loss), compared to the 0D case, $\frac{|F_{\pm3}[a_d,a_{\rm latt},Z]|}{|F_\perp[a_d,a_{\rm latt},Z]|} \gtrsim \frac{|f_{-3}[a_d,Z]|}{|f_\perp[a_d,Z]|}$ which results in larger nonadiabatic loss rates.

For the 1D potential, using the fields in Eq. (34) we solve the equivalent of equation Eq. (13) within the cell q. Following Eq. (16), the lowest energy trapped state is

$$|t^j;\ell;N;\mathcal{N}=1\rangle_q = |t_q,\ell N\rangle\,|\mathcal{N}=1,-,\varphi_q\rangle\,,$$
$$\langle\tilde{\vec{R}}_q\ |\ t_q,\ell N| = \frac{\sqrt{2}(\tilde{R}_q)^{\ell_{\rm eff}}\exp\left[-\tilde{R}_q^2/2\right]\mathcal{L}_N^{\ell_{\rm eff}}\left[\tilde{R}_q^2\right]}{(\Gamma[N+\ell_{\rm eff}+1]/N!)^{1/2}}, \tag{35}$$

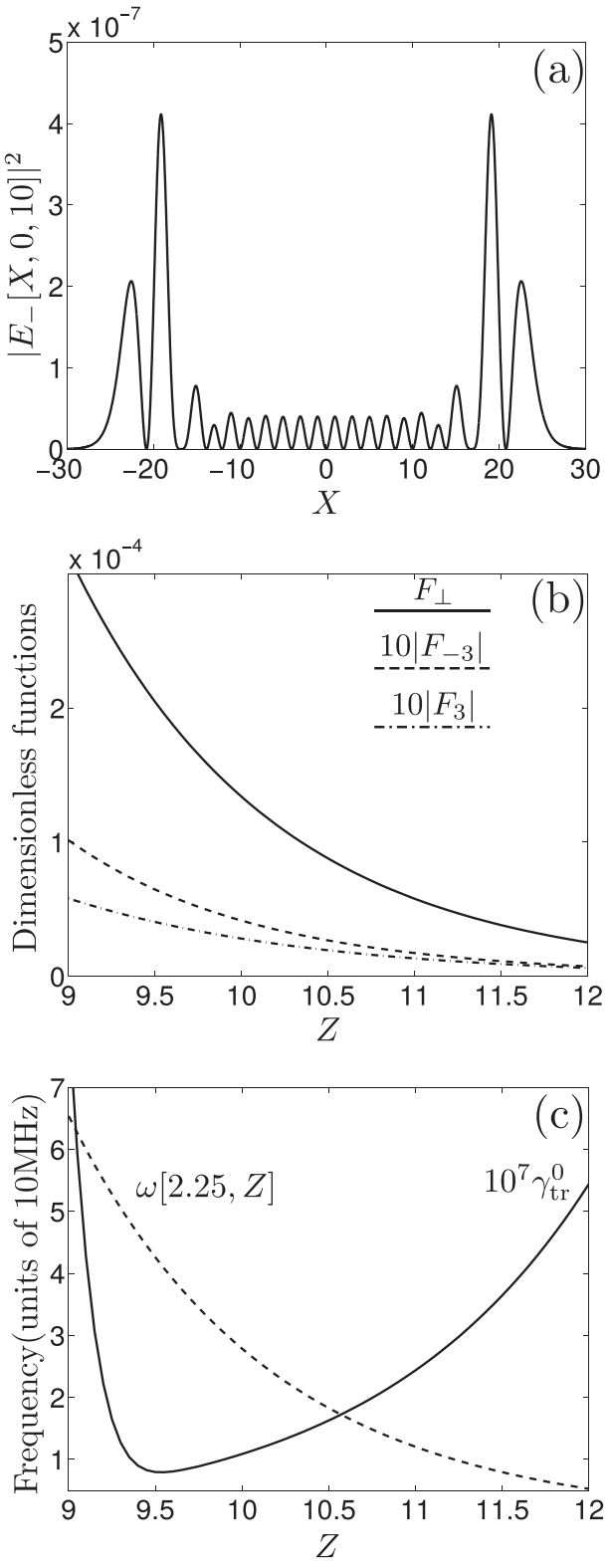

FIG. 7. (a) Shape of the trap potential due to the azimuthal field for a lattice with $N_f = 10$, $a_d = 2.25$, and $a_{\rm latt} = 2a_d$. (b) Plot of fitting parameters F_η defined in Eq. (34): $F_\perp[2.25,4.5,Z]$ (solid line), $10F_3[2.25,4.5,Z]$ (dash-dotted line), and $-10F_{-3}[2.25,4.5,Z]$ (dashed line). (c) The dashed line represents the zero-point trap frequency $\omega[2.25,4.5,Z]/2$ in units of 10 MHz. The solid line is $10^7\gamma^0_{\rm tr}$, the total molecule loss rate for the $j = 0$ hyperfine state (in Hz).

where $\vec{\tilde{R}}_q = \vec{\tilde{R}} - q\tilde{a}_{\rm latt}\hat{X}$, with $\tilde{a}_{\rm latt} = a_{\rm latt}/\sigma[a_d,a_{\rm latt},Z]$, and the Z-dependent oscillator width and frequency have the form

$$\sigma^2[a_d,a_{\rm latt},Z] = \frac{(10K\hbar B_e)^{1/2}}{F_\perp[a_d,a_{\rm latt},Z]\alpha_{\rm mf}},$$
$$\hbar\omega[a_d,a_{\rm latt},Z] = |\alpha_{\rm mf}|F_\perp[a_d,a_{\rm latt},Z]\left(\frac{2K}{5\hbar B_e}\right)^{1/2}. \quad (36)$$

We plot the trap frequency for the parameters in Tables I and II in Fig. 7(c) (the dashed line).

A. Z trapping in 1D

To prevent the molecule from escaping in the Z direction, we use the same laser setup as discussed in Sec. V A. As an example, from Fig. 7(c), an optimum position to trap the molecule will be around $Z = 9.5$ where the trap frequency $\omega[2.25,4.5,9.5] \approx 10$ MHz. To look for laser parameters, we use Eq. (23) as an expression for an effective potential along the Z axis with $Z_1 \approx 9.5$. This is fulfilled for a total laser power $I_0 = 1.0\,{\rm MW\,cm^{-2}}$ and the focal plane $Z_0 = 7.65$. The corresponding Z-axis trap frequency $\omega_Z = 0.5$ MHz and oscillator length $\sigma_Z = 0.2$. Though the Z trapping is much weaker than the radial trapping, the oscillator length is still less than the nanorod radius. One important change from the 0D case is the laser induced loss rate, which will be around $\approx$1 s.

B. Molecular loss rate

Now, we estimate the molecular loss rate for 1D by following similar procedures as discussed in Sec. VI with the fitting functions denoted by f replaced by the corresponding 1D functions, F. For each cell, we calculate the 1D equivalent of the molecular loss rate following the treatment for Eqs. (25) and (26). The total molecule loss rate for the $j = 0$ state ($\gamma^0_{\rm tr}$) is shown in Fig. 7(c). For the 1D case, the calculation of the nonadiabatic loss rates due to the R^4 potential gives results similar to Eqs. (25) and (26), with $F_{\pm3}$ in place of f_{-3}. Again, we notice the interplay between nonadiabatic loss ($\propto \omega^{-1}[a_d,a_{\rm latt},Z]$) and hyperfine-induced molecule loss ($\propto\omega[a_d,a_{\rm latt},Z]$). Because of the relatively large nonadiabatic coupling (compared to 0D), controlled by the ratio $\frac{|F_{\pm3}[a_d,a_{\rm latt},Z]|}{|F_\perp[a_d,a_{\rm latt},Z]|}$, we need a high trap frequency to minimize the nonadiabatic loss rate. The hyperfine-induced loss rate is controlled by the potential barrier between the $j = 0,1$ hyperfine states: $|E_0 - E_1|/\omega[a_d,a_{\rm latt},Z]$, which in turn is controlled by the magnetic field. Accordingly, we need a stronger magnetic field, see Table III, to increase the potential barrier between the hyperfine states. The minimum loss rate we obtain for the parameters in Table III: $\gamma^0_{\rm tr} \approx 0.8{\rm s}^{-1}$ for $Z \approx 9.5$. One way to increase lifetime will be by increasing a_d or $a_{\rm latt}$, which will result in increased lattice constant and lower the energy scales.

Moreover, as we are in a lattice, we like to have a stable local trap; i.e., we want to have a small tunneling rate, which is guaranteed as long as $a_{\rm latt}/\sigma \gg 1$ [7]. From Eq. (36), we see that the ratio $a_d/\sigma \sim |F_\perp[a_d,a_{\rm latt},Z]|a_{\rm mf}$, where $F_\perp[a_d,a_{\rm latt},Z]$ is weaker than the corresponding 0D fitting function $f_\perp[a_d,a_{\rm latt},Z]$ for fixed $a_d,a_{\rm latt},Z$. As a result, we

need to increase the ferroelectric strength $\alpha_{\rm mf}$ to get the same $a_{\rm latt}/\sigma[a_d,a_{\rm latt},Z]$. Therefore, we chose in Table I the polarization strength for 1D stronger than that of 0D. Consequently, one needs to use ferroelectric material with high spontaneous polarization like PZT (lead zirconate titanate compounds). For such parameters, we find that $a_{\rm latt}/\sigma[2.25,5,9.5] \sim 10^2$, which implies an effectively vanishing tunneling rate.

Next we consider the substrate-induced loss rate as discussed in Sec. VII. Compared to the 0D case, the trap center is closer to the surface at $Z \approx 9.5$. As a result, for the parameters in Table I, we obtain from Eq. (28) a loss rate $\gamma_h \sim 0.2\,{\rm s}^{-1}$. We also obtain a similar loss rate for phonon induced noise from Eqs. (32). From these discussion it is clear that the most important loss mechanism originates from nonadiabatic and hyperfine coupling with molecule lifetime on the order of 1 s [Fig. 7(c).

IX. SIMULATION OF QUANTUM SPIN MODEL

From the discussion in the previous section, it is clear that each primitive cell of the ferroelectric lattice can trap molecules. For the $\mathcal{N}=1$ manifold, the trapped state at a site q is given by Eq. (35). By applying a laser field similar to Sec. V A, we trap the molecule at $Z=Z_0$.

To use the molecules as spins, we need a second trapped state. We have carried out similar studies as in the previous sections for the level $\mathcal{N}=2$. Let $|{\pm}1\rangle$ again denote the $\mathcal{M}_\mathcal{N}=\pm1$ projection on the molecular axis. The quadratic Stark shift for $\mathcal{N}=2$ level is weaker than for $\mathcal{N}=1$. Numerically, we find that the effective potential [Eq. (11)] is $V_{\rm rad}^{\mathcal{N}=2} \approx V_{\rm rad}^{\mathcal{N}=1}/4$. We then solve the equivalent of Eqs. (13), (14), and (F2), only changing the potential strength. We denote the transverse trapping width for $\mathcal{N}$ manifold as $\sigma_\mathcal{N}[a_d,Z]$. In relation to the oscillator width and energy for the $\mathcal{N}=1$ state, $\sigma_2[a_d,a_{\rm latt},Z] \approx \sqrt{2}\sigma_1[a_d,a_{\rm latt},Z]$ and $\omega_2[a_d,a_{\rm latt},Z] = \omega_1[a_d,a_{\rm latt},Z]/2$. For the laser-induced potential, as noted in Ref. [33], the polarizability of the molecule is almost independent of $\mathcal{N}$ and as a result we trap the $\mathcal{N}=2$ state also at Z_0. Following Eq. (35), the corresponding trapped state is then expressed as

$$|t^j;\ell;N;\mathcal{N}=2\rangle_q = |t'_q,\ell N\rangle\,|\mathcal{N}=2,-,\varphi_q\rangle\,,$$
$$\langle\vec{\tilde{R}}_q \mid t'_q,\ell N\rangle = \frac{\sqrt{2}(\tilde{R}_q)^{\ell_{\rm eff}}\exp\left[-\tilde{R}_q^2/4\right]\mathcal{L}_N^{\ell_{\rm eff}}\left[\tilde{R}_q^2/2\right]}{2^{\ell_{\rm eff}/2}(\Gamma[N+\ell_{\rm eff}+1]/N!)^{1/2}}. \tag{37}$$

For this section, we only consider the motional states $\ell=0,N=0$ and as a result omit these labels in our description of the states. To simulate a spin model with long-range dipolar interaction, we first consider just two cells at q and q' and assume that each cell is filled with one molecule in the state $|t^0;\mathcal{N}=1\rangle$ or $|t^0;\mathcal{N}=2\rangle$. We introduce the spin operators,

$$\boldsymbol{S}_q^+ = |t^0;1;0;\mathcal{N}=2\rangle_q\,\langle t^0;1;0;\mathcal{N}=1|_q\,,$$
$$\boldsymbol{S}_q^z = \sum_{\eta=1,2}(-1)^\eta\,|t^0;1;0;\mathcal{N}=\eta\rangle_q\,\langle t^0;1;0;\mathcal{N}=\eta|_q\,, \tag{38}$$

and $\boldsymbol{S}_q^- = [\boldsymbol{S}^+]_q^\dagger$. The dipole-dipole Hamiltonian projected to the subspace of interest is then given by

$$H_{\rm class} = V_{\rm dd}\sum_{q\neq q'}\frac{\boldsymbol{S}_q^+\boldsymbol{S}_{q'}^- + (\boldsymbol{S}_q^+\boldsymbol{S}_{q'}^+ + \boldsymbol{S}_q^-\boldsymbol{S}_{q'}^-)/2}{|q-q'|^3} + 4\hbar B_e\sum_q \boldsymbol{S}_q^z, \tag{39}$$

where dipolar energy is given by

$$V_{\rm dd} = \frac{\mu^2\sum_{\mathcal{M}_\mathcal{N}=\pm1}|\langle\mathcal{N}=1,\mathcal{M}_\mathcal{N}|\boldsymbol{T_0^1}|\mathcal{N}=2,\mathcal{M}_\mathcal{N}\rangle|^2}{8\pi\epsilon_0 a_{\rm latt}^3}, = \frac{1}{5}\frac{\mu^2}{4\pi\epsilon_0 a_{\rm latt}^3}, \tag{40}$$

with the factor of $1/5$ originating from the dipole matrix between the $\mathcal{N}=1$ and $\mathcal{N}=2$ states and the last term denoting detuning between the two spin states. For the parameters concerned, $V_{\rm dd} \ll \hbar B_e$, $\boldsymbol{S}_q^z$ becomes a conserved quantity and as a result, the pair creation and annihilation terms $\boldsymbol{S}_q^+\boldsymbol{S}_{q'}^+, \boldsymbol{S}_q^-\boldsymbol{S}_{q'}^-$ in Eq. (40) are suppressed. Hence, one has a long-range classical Ising model.

To simulate a quantum model, one way is to couple the $|t^0;1;0;\mathcal{N}=2\rangle_q$, $|t^0;1;0;\mathcal{N}=1\rangle_q$ state by introducing a linearly Z-polarized time-periodic microwave field $\vec{E}_{\rm mw} = \mathcal{E}\cos\Omega t\,\hat{Z}$, where $\Omega = 4B_e+\Delta$. The microwave coupling Hamiltonian is given by $H_{\rm mw} = g_{\rm mw}\cos\Omega t\sum_q \boldsymbol{S}_q^x$, where $g_{\rm mw} = \frac{\mu\mathcal{E}}{\sqrt{5}}\langle t'_q,10\mid t_q,10\rangle$. Going to the rotating frame and projecting to the trapped state, the spin Hamiltonian has the form (see Appendix J)

$$H_{\rm spin} = V_{\rm dd}\sum_{q,q'}\frac{\boldsymbol{S}_q^+\boldsymbol{S}_{q'}^-}{|q-q'|^3} + \hbar(\Delta-\omega_1[a_d,Z_0]/2)\sum_q\boldsymbol{S}_q^z + g_{\rm mw}\sum_q\boldsymbol{S}_q^x. \tag{41}$$

The second term in Eq. (41) originates from the detuning of the microwave field and the difference in trap frequency of the two trapped states. The microwave-molecule coupling gives the last term, where we have assumed that the width of the wave function in Z remains the same in both levels. The Hamiltonian in Eq. (41) is an example of a long-range XX spin Hamiltonian in a transverse and longitudinal field, both of which are tunable.

Note, however, that the presence of more than one molecule and the dipolar interactions also lead to a new loss mechanism: Dipolar collisions between two molecules can also resonantly couple the states $|t;\mathcal{N}=2\rangle_q\,|t;\mathcal{N}=1\rangle_{q'}$ to the untrapped states $|\mathcal{N}=2,\mathcal{M}_\mathcal{N}=0\rangle\,|\mathcal{N}=1,\mathcal{M}_\mathcal{N}=0\rangle$, where q,q' are two sites in the lattice. As discussed in Sec. V A, the $\mathcal{M}_\mathcal{N}=0$ state is detuned from the $\mathcal{M}_\mathcal{N}=\pm1$ state. As a result, the loss rate is suppressed by a factor (see Appendix J) of

$$\left(V_{\rm dd}^2/K\right)\exp\left[-2\frac{\alpha_0 I_0}{K}\right]. \tag{42}$$

For a laser strength of $I_0 \sim 1.0\ {\rm MW\,cm^{-2}}$ and the polarizability taken from Ref. [38], and using parameters from Table I, we find that $\alpha_0 I_0/K \sim 10^2$. We see that such a loss rate is exponentially suppressed.

Moreover, to suppress motional excitation, one needs to make sure that the dipolar energy remains much weaker than the local trap energy: $V_{\rm dip} < 2\hbar\omega[a_d, a_{\rm latt}, Z]$. This gives a lower limit on the lattice constant $a_{\rm latt}$ for a fixed molecule and ferroelectric polarization. For the parameters in Tables I and II with a molecule trapped at $Z_0 = 9.5$ [minimum loss rate from Fig. 7(c)], we find that the dipolar energy $V_{\rm dip} \approx 6\,$kHz which is small compared to the trap energy of $\sim$1 MHz. Moreover, as our trap is stable for around $\sim$1 s, such a dipolar coupling in principle allows us to perform around $V_{\rm dip}/\min[\gamma_{\rm tr}^0] \approx 7 \times 10^3$ gate operations. If we use instead a 5T magnetic field to suppress the hyperfine loss, we can gain an order of magnitude in the number of gate operations by decreasing the nanorod radius $r_d = 20\,$nm. For a comparison to a possible optical lattice trap, we assume a setup similar to Ref. [14] with an additional microwave field to couple $|\mathcal{N}=0, \mathcal{M}_\mathcal{N}=0\rangle$ to $|\mathcal{N}=1, \mathcal{M}_\mathcal{N}=0\rangle$. The resulting spin model permits gate operation of order $\sim 3 \times 10^2$. Thus, in our setup we can expect an increase in the number of potential gate operations by a factor of $\sim$20.

X. SUMMARY AND CONCLUSIONS

In summary, we have proposed nanotraps for polar molecules near an array of ferroelectric nanorods. Our most important finding is that in the proposed scheme there exist trapped states with suppressed molecular loss rate even within the regime of nanoscale confinement. The molecules are held at a certain distance from the nanorods by the combined potentials of the nanorods and a standing-wave laser field. Moreover, we have shown that the trapping scheme can be extended to a one-dimensional periodic structure with lattice constant $\sim$200 nm. We carried out a qualitative analysis of the main loss mechanisms, including nonadiabatic losses as well as hyperfine-, laser-, and surface-induced losses. Considering, in particular, RbCs molecules that have already been prepared at temperatures below those corresponding to our trap, we find that the main limiting process comes from the interplay between nonadiabatic and hyperfine coupling and leads to a lifetime of $\sim$10 s for 0D trap and $\sim$1 s for 1D trap. This time, in principle, can be increased by applying a stronger static magnetic field. As an application, we have sketched a way to simulate a family of long-range spin Hamiltonians using our proposed 1D array of traps.

We like to point out that the present proposal can be applied to all $^1\Sigma$ diatomic molecules. Depending on the hyperfine and rotational structure of the molecule, the dependence of the loss rate on the magnetic field will change. Moreover, one can exploit the possibility that for $\mathcal{N} > 1$, there can be more than one trapped state which can lead to more exotic spin models. In addition, a difference in trapping properties between different $\mathcal{N}$ manifolds can be exploited to generate spin models by shaking the Z-axis optical potential without using a microwave field.

While our proposal combining electrostatic with optical trapping is restricted to 1D arrays, we note that a 2D geometry can be realized by using a two-dimensional arrangement of the purely electrostatic 0D traps presented in Fig. 5, in which there is no limitation due to optical trapping. Moreover, as no special optical properties of the molecule are required, such a scheme can, in principle, be used to trap general rigid-rotor-like molecules.

More generally, the use of nanostructures for trapping polar molecules opens several new directions. One possible extension is to investigate its potential for trapping other types of molecules such as, e.g., those of $^2\Sigma$ type, which have a richer fine structure due to an unpaired electron spin. Furthermore, ferroelectrics in the nanoregime can have exotic (e.g., vortexlike) polarization distribution [44,45], which can be controlled in dynamical manner. Such control can potentially give rise to a *state-independent* trap in a time-averaged potential. Another direction will be to extend our trapping scheme to open shell molecules, e.g., $^2\Sigma$ molecules. Such molecules have a magnetic moment and can then be trapped by ferro*magnetic* nanorods [46]. Moreover, ferromagnetic states can be switched in nanosecond rates [47], allowing for fast, time-dependent potentials, which can again give rise to a novel state-independent mechanism to trap open-shell molecules.

Another route of further investigation will focus on the usability of such traps for quantum information processing and for precision measurements.

ACKNOWLEDGMENTS

We acknowledge interesting discussions with M. Zeppenfeld. G.G. acknowledges support by the Departamento de Educación del Gobierno Vasco through Project No. PI-2016-1-0041.

APPENDIX A: SYMMETRIES OF THE TRAPPING POTENTIAL

We consider the simplest ferroelectric trapping geometry consisting of only four nanorods, i.e., $N_f = 1$, corresponding to just one square in Fig. 1 as outlined by the dashed line. The symmetry of the arrangement of ferroelectrics gives useful insight into the properties of the electric field. There are three relevant symmetries $R_J, J = 1,\ldots,3$ involved: reflection at $Y = 0$, reflection at $X = 0$, and rotation around Z by $\pi/2$. Each of these operations moves a $\pm$ polarized nanorod to a $\mp$ polarized one. Therefore, the electric field $\vec{E}(\vec{R})$ changes sign under each of the symmetry transformations R_J, i.e., [48],

$$R_J \vec{E}\left(R_J^{-1}\vec{R}\right) = -\vec{E}(\vec{R})\ \forall J = 1,\ldots,3. \tag{A1}$$

We are interested at the field distribution close to the origin (the center between the rods) but outside of the volume containing the nanorods. Thus, we can use a Taylor series in X, Y for each component of $\vec{E}$,

$$E_u(X,Y,Z) = \sum_{n,m\geqslant 0} c^u_{nm}(Z) X^n Y^m, \quad u = X,Y,Z. \tag{A2}$$

Then from R_1 (reflection at $Y = 0$), we obtain

$$\begin{pmatrix} -E_X(-X,Y,Z) \\ E_Y(-X,Y,Z) \\ E_Z(-X,Y,Z) \end{pmatrix} = -\vec{E}(X,Y,Z),$$

which implies $c^X_{nm} = (-1)^n c^X_{nm}$ and $c^Y_{nm} = -(-1)^n c^Y_{nm}$, i.e.,

$$c^X_{nm} = 0\,\forall n \text{ odd}, \quad c^Y_{nm} = 0\,\forall n \text{ even}, \quad c^Z_{nm} = 0\,\forall n \text{ even}. \tag{A3}$$

Similarly, reflection at $X = 0$ yields

$$c^X_{nm} = 0\,\forall m \text{ even}, \quad c^Y_{nm} = 0\,\forall m \text{ odd}, \quad c^Z_{nm} = 0\,\forall m \text{ even}. \tag{A4}$$

Thus, we can conclude that the only nonzero terms in the Taylor series are $c^X_{\text{odd,even}}, c^Y_{\text{even,odd}}$, and $c^Z_{\text{even,even}}$. Note that these symmetries persist even in the 1D case and thus still apply to the (center of) the 1D array of nanorods. R_3, in contrast, only holds for the 0D case (and would be restored for the (center of) a full 2D arrangement that we do not discuss here):

$$c^X_{nm} = -(-1)^m c^Y_{mn}, \tag{A5}$$

$$c^Y_{nm} = +(-1)^m c^X_{mn}, \tag{A6}$$

$$c^Z_{nm} = -(-1)^m c^Z_{mn}. \tag{A7}$$

We are mainly interested in the *azimuthal* field component $E_- = E_X - iE_Y$. Inserting the Taylor series for $E_{X,Y}$ and expressing X and Y in polar coordinates, we find

$$E_-(R,\varphi,Z) = \sum_{n,m} \left[c^X_{nm}(Z) - i c^Y_{nm}(Z)\right] R^{n+m} \cos^n\varphi \sin^m\varphi.$$

Using that both c^X_{nm} and c^Y_{nm} vanish whenever $n+m$ is even, we see that only odd powers of R appear in the series and only powers of $e^{il\phi}$ with $|l| < 2k1$ appear. Therefore, we are justified to make the ansatz

$$E_-(R,\varphi,Z) = \sum_{k\geqslant 0, 2k+1\geqslant |l|} c^-_{kl}(Z) R^{2k+1} e^{il\varphi} \equiv \sum_l c^-_l(Z,R) e^{il\varphi}, \tag{A8}$$

where the $c^-_l(Z,R)$ are odd functions of R. While further constraints on l can be obtained (after some algebra) by relating c^X, c^Y, and c^-, they are easier to see by applying the symmetry operations directly to the Fourier series of E_- and using that from the three symmetry operations, we get

$$E_-(X,Y,Z) = E^*_-(-X,Y,Z) \equiv E^*_-(R,\pi-\varphi,Z), \tag{A9}$$

$$= -E^*_-(X,-Y,Z) \equiv -E^*_-(R,-\varphi,Z), \tag{A10}$$

$$= iE_-(Y,-X,Z) \equiv iE_-(R,\varphi-\pi/2,Z). \tag{A11}$$

This implies that $c^-_l = (c^-_l)^* e^{il\pi} = (c^-_l)^* e^{i\pi} = c^-_l e^{-i(m-1)\pi/2}$, from which we conclude that

$$c^-_l = 0\,\forall l \neq 4J+1, \tag{A12}$$

$$c^-_l = -(c^-_l)^*, \tag{A13}$$

i.e., only c^-_l with $l = \ldots, -3, 1, 5, \ldots$ may be nonzero (neither even powers of $e^{i\varphi}$ in the Fourier series of E_- nor powers $4k-1$).

Analogously, we find for the Fourier series of $E_Z(\varphi,R,Z) = \sum_l c^Z_l(R,Z)e^{il\varphi}$ that $-c^Z_l = e^{il\pi}c_{-l} = c^Z_{-l} = e^{il\pi/2}c^Z_l$, from which we conclude that c^Z_l may be nonzero only for $l = 4J+2$ and that $c^Z_{-l} = -c^Z_l$; all c^Z_l are *even* functions of R.

Note that these considerations only apply to 0D case or the center of a 1D or 2D array. However, due to the diminishing influence of the boundary, it will approximately hold also for cells close to the center of such an array.

APPENDIX B: NONADABATIC CONTRIBUTION TO POTENTIAL EQ. (8)

Here, we consider the nonadiabatic effect to the Hamiltonian due to the position dependence of the perturbation in Eq. (8). The second-order energy corrections arise from a first-order correction to the unperturbed states. The transformed states related to our model are given by (we neglect the hyperfine structure for this discussion)

$$\begin{aligned}
|\tilde{0},\tilde{0}\rangle &= |\mathcal{N}=0,\mathcal{M}_\mathcal{N}=0\rangle - \sum_{\substack{\mathcal{N}'>0,\\ \mathcal{M}_{\mathcal{N}'}}} \frac{\langle \mathcal{N}',\mathcal{M}_{\mathcal{N}'}|\, H_{\text{mf}}\, |\mathcal{N}=0,\mathcal{M}_\mathcal{N}=0\rangle}{\hbar B_e \mathcal{N}'(\mathcal{N}'+1)} |\mathcal{N}',\mathcal{M}_{\mathcal{N}'}\rangle,\\
&= |\mathcal{N}=0,\mathcal{M}_\mathcal{N}=0\rangle + \frac{\alpha_{\text{mf}}}{2\sqrt{6}\hbar B_e}(E_-\,|\mathcal{N}=1,\mathcal{M}_\mathcal{N}=1\rangle + E_+\,|\mathcal{N}=1,\mathcal{M}_\mathcal{N}=-1\rangle),\\
|\tilde{1}\rangle &= |\mathcal{N}=1,\mathcal{M}_\mathcal{N}=1\rangle + \sum_{\substack{\mathcal{N}'\neq 1,\\ \mathcal{M}_{\mathcal{N}'}}} \frac{\langle \mathcal{N}',\mathcal{M}_{\mathcal{N}'}|\, H_{\text{mf}}\, |\mathcal{N}=1,\mathcal{M}_\mathcal{N}=1\rangle}{\hbar B_e(2-\mathcal{N}'^2-\mathcal{N}')} |\mathcal{N}',\mathcal{M}_{\mathcal{N}'}\rangle,\\
&= |\mathcal{N}=1,\mathcal{M}_\mathcal{N}=1\rangle - \frac{\alpha_{\text{mf}}}{4\sqrt{5}\hbar B_e}\left(E_-\,|\mathcal{N}=2,\mathcal{M}_\mathcal{N}=2\rangle + \frac{E_+}{\sqrt{6}}\,|\mathcal{N}=2,\mathcal{M}_\mathcal{N}=0\rangle - \sqrt{\frac{10}{3}}E_+\,|\mathcal{N}=0,\mathcal{M}_\mathcal{N}=0\rangle\right),\\
|-\tilde{1}\rangle &= |\mathcal{N}=1,\mathcal{M}_\mathcal{N}=-1\rangle + \sum_{\substack{\mathcal{N}'\neq 1,\\ \mathcal{M}_{\mathcal{N}'}}} \frac{\langle \mathcal{N}',\mathcal{M}_{\mathcal{N}'}|\, H_{\text{mf}}\, |\mathcal{N}=1,\mathcal{M}_\mathcal{N}=-1\rangle}{\hbar B_e(2-\mathcal{N}'^2-\mathcal{N}')} |\mathcal{N}',\mathcal{M}_{\mathcal{N}'}\rangle,\\
&= |\mathcal{N}=1,\mathcal{M}_\mathcal{N}=-1\rangle - \frac{\alpha_{\text{mf}}}{4\sqrt{5}\hbar B_e}\left(E_+\,|\mathcal{N}=2,\mathcal{M}_\mathcal{N}=-2\rangle + \frac{E_-}{\sqrt{6}}\,|\mathcal{N}=2,\mathcal{M}_\mathcal{N}=0\rangle - \sqrt{\frac{10}{3}}E_-\,|\mathcal{N}=0,\mathcal{M}_\mathcal{N}=0\rangle\right).
\end{aligned} \tag{B1}$$

The nonadiabatic effect then can be estimated by employing the kinetic energy operator onto the states $|\tilde{0},\tilde{0}\rangle$, $|\pm\tilde{1}\rangle$. As we have seen that the width of the trapped states are within the linear region of the electric field strength, we only consider the effects of $E_\pm$ fields. The resulting kinetic operator reads $K_{\rm tot} = K_0 + K_1 + K_2$, where

$$K_0 = K(|\tilde{0},\tilde{0}\rangle\langle\tilde{0},\tilde{0}| + |\tilde{1}\rangle\langle\tilde{1}| + |-\tilde{1}\rangle\langle-\tilde{1}|)\nabla^2,$$

$$K_1 = K\left(\frac{\alpha_{\rm mf}}{2\sqrt{6}\hbar B_e}\right)^2 \sum_{\sigma=\pm}(E_\sigma(\nabla E_\sigma)(\nabla|\tilde{0},\tilde{0}\rangle)\langle\sigma\tilde{1}| + E_{-\sigma}(\nabla E_{-\sigma})(\nabla|\sigma\tilde{1}\rangle)\langle\tilde{0},\tilde{0}| + E_{-\sigma}(\nabla E_\sigma)\cdot(\nabla|\tilde{0},\tilde{0}\rangle)\langle\tilde{0},\tilde{0}|), \tag{B2}$$

$$K_2 = K\left(\frac{\alpha_{\rm mf}}{4\sqrt{30}\hbar B_e}\right)^2 \sum_{\sigma=\pm}(E_{-\sigma}(\nabla E_{-\sigma})(\nabla|\sigma\tilde{1}\rangle)\langle-\sigma\tilde{1}| + E_\sigma(\nabla E_{-\sigma})(\nabla|\sigma\tilde{1}\rangle)\langle\sigma\tilde{1}|),$$

where a derivative on a internal state is used as a expression for derivative on the position wave function of that internal state. The first term, Eq. (B2), is the adiabatic part of the kinetic operator. K_1 denotes the nonadiabatic contribution and couples the $\mathcal{N}=1$ states to $\mathcal{N}=0$ level. Such a transition has energy gap of $\hbar B_e$. In the present case, we find that $\|K_1\|/(\hbar B_e) \sim 10^{-7}$ and as a result its effect can be neglected. The operator K_2 in Eq. (B2) denotes nonadiabatic corrections leading to coupling between the trapped states. In the linear field regime, ($E_- \propto -ie^{i\varphi}$), this term can be shown to be proportional to $(\nabla|-\varphi\rangle)\langle-\varphi|$. Again as $\|K_2\|/K \sim 10^{-4}$, we can neglect its effect compared to the adiabatic contribution.

Similarly, one can show that the nonadiabatic coupling between the other states also results in small corrections to the kinetic operator.

APPENDIX C: LOSS DUE TO HYPERFINE STRUCTURE INDUCED COUPLING

We give the detailed derivation of the hyperfine structure induced loss rates as presented in Sec. VI B. The loss rate arises due to the off-diagonal elements of H_{01}, H_{10} in Eq. (14) which are of order $\delta \ll 1$ (cf. Table III) and couple each trapped state to a continuum state with different hyperfine structure. We are interested in a regime where the energy of $j=0$ trapped state $2\omega[a_d,Z] - |E_0 - E_1| < 0$. Moreover, we are interested in a regime where the width of the trapped state is much smaller than the classical turning point radius. Away from the size of our square cell, $R > a_d/2$, we assume that the untrapped state is essentially a free particle with respective energy-independent two-dimensional density of states. Assuming such density of state is an approximation which can drastically change in presence of a resonance. In such cases, one can use the magnetic field to tune $|E_0 - E_1|$ away from such a resonance.

The relevant equations for the $j=0$ trapped state are derived from Eqs. (13) and (14),

$$\begin{bmatrix} -\left(\partial_{\tilde{R}}^2 + \frac{\partial_{\tilde{R}}}{\tilde{R}} - \frac{1}{\tilde{R}^2}\right) + \tilde{R}^2 - \frac{2E_0}{\hbar\omega[a_d,Z]} & -\frac{3\delta\tilde{R}^2}{4} \\ -\frac{3\delta\tilde{R}^2}{4} & -\left(\partial_{\tilde{R}}^2 + \frac{\partial_{\tilde{R}}}{\tilde{R}} - \frac{5}{\tilde{R}^2}\right) + V[\tilde{R}] - \frac{2E_0}{\hbar\omega[a_d,Z]} \end{bmatrix} = \frac{2\epsilon}{\hbar\omega[a_d,Z]} \begin{bmatrix} t_1^0[\tilde{R}] \\ u_{-1}^1[\tilde{R}] \end{bmatrix}. \tag{C1}$$

We are interested in a region where $|E_0 - E_1| > 2\omega[a_d,Z]$, i.e., where resonant tunneling is possible when the energy of the continuum state is $\epsilon_{\rm res} = 2\omega[a_d,Z] - |E_0 - E_1|$. This corresponds to a situation where the center of the trap $R=0$ is situated in a classically forbidden region of the continuum state.

We first numerically calculate the position dependence of $|u^1,-1\rangle$ with energy $\epsilon_{\rm res}$ where we replace the shape of the potential for the continuum state as $V[\tilde{R}] = -\tilde{R}^2/2, \tilde{R} < \tilde{a}_d/2$ and $V[\tilde{R}] = V[\tilde{a}_d/2] = -\tilde{a}_d^2/8, \tilde{R} \geqslant \tilde{a}_d/2$. The reason behind this substitution is that the potential for the continuum state has a downward curvature near the center of the trap with the minimum residing at the boundary of the square cell. Our trapped states are concentrated near the center of the square cell ($\sigma[a_d,Z]/a_d \ll 1$) and we are interested in classically forbidden energy regimes $\epsilon \sim V[a_d/2]$. With this substitution, we find the solution for $|u^1,-1\rangle$ inside a region of $\tilde{R} \in [0,\tilde{R}_{\rm max}]$. To find the density of states at the resonant energy, we first notice that as $\tilde{R} \to \infty$, the solution should approach the free-particle wave function $\propto \mathcal{J}_{\sqrt{5}}[\alpha_M \tilde{R}/\tilde{R}_{\rm max}]$, where α_M is the Mth zero of the Bessel function $\mathcal{J}_{\sqrt{5}}[x]$. Here, we numerically find M_0 by maximizing the overlap function: $O[M] = |\langle M \mid u^1,-1\rangle|^2$ where $|M\rangle = \sqrt{2}\tilde{R}_{\rm max}^2 \mathcal{J}_{\sqrt{5}}[\alpha_M \tilde{R}/\tilde{R}_{\rm max}]/\mathcal{J}_{\sqrt{5}+1}[\alpha_M]$. The density of states is then given by $\mathcal{D}[M_0] = \tilde{R}_{\rm max}^2/(2\pi\alpha_{M_0})$. Then using Fermi's golden rule, we express the transition rate from the lowest energy trapped state to the continuum as

$$\frac{\gamma_{\rm hf}^0}{\hbar\omega[a_d,Z]} = \frac{9\pi\delta^2\mathcal{D}[M_0]}{32}|\langle u^1,-1|\tilde{R}^2|t^0,01\rangle|^2. \tag{C2}$$

On the other hand, the transition rate from the trapped state $|t^1,01\rangle$ happens at a positive energy and is given by

$$\frac{\gamma_{\rm hf}^1}{\hbar\omega[a_d,Z]} = \frac{9\pi\delta^2\mathcal{D}[M_{\rm res}]}{32}|\langle u^0,3|\tilde{R}^2|t^1,01\rangle|^2, \tag{C3}$$

where the resonant condition now reads $\alpha_{\ell,M_{\rm res}}^2/\tilde{R}_0^2 = 4 + 2|E_0 - E_1|/(\hbar\omega[a_d,Z]) + \tilde{R}^2/2$; cf. Sec. VI B.

APPENDIX D: LOSS RATE DUE TO THE R^3 DEPENDENCE OF ELECTRIC FIELD

1. Loss rate for 0D trap

Including the correction due to $\propto R^3\exp[-3i\varphi]$ in Eq. (10) and going to the transformed basis, the equation of motion for

the $\ell = 1$ trapped state Eq. (15) reads

$$\frac{-1}{2}\left(\partial_{\tilde{R}}^2 + \frac{\partial_{\tilde{R}}}{\tilde{R}} - \frac{1}{\tilde{R}^2} - 2\tilde{R}^2\right) t_1^j[\tilde{R}] + \frac{f_{-3}[a_d,Z]K}{f_\perp[a_d,Z]\omega[a_d,Z]} \times \tilde{R}^4 \sum_{\eta=\pm1}\left(t_{1+4\eta}^i[\tilde{R}] - \frac{3}{4}u_{1+4\eta}^j[\tilde{R}]\right) = \frac{\epsilon_1 + E_i}{\hbar\omega[a_d,Z]} t_1^j[\tilde{R}], \tag{D1}$$

where $\tilde{R} = R/\sigma[a_d,Z]$ and the last term on the right-hand side arises from the R^3 correction to the field. While deriving Eq. (D1), we have neglected the effect of $f_{1\perp}[a_d,Z]$ in Eq. (10), as we consider regions with $N_{\max} > 1$ where its effect is negligible as it only renormalizes the trapping frequency by a factor $1 + (f_{1\perp}[a_d,Z]/f_\perp[a_d,Z])^2 \approx 1$ (cf. Fig. 3). As a result, we only consider the effect of $f_{-3}[a_d,Z]$ components in Eq. (10). Next, we solve Eq. (D1) perturbatively with the zeroth-order solution given by Eq. (16). The second last term in Eq. (D1) couples $j,1,N$ to $|t_{-3N'}^1\rangle$, $|t_{5N'}^1\rangle$ states. As from Fig. 3, $|f_{-3}[a_d,Z]|/f_\perp[a_d,Z] \sim 10^{-3}$, we express the perturbed wave function as

$$|\underline{t}^j,1N\rangle = |t^j,1N\rangle + \frac{f_{-3}[a_d,Z]K}{f_\perp[a_d,Z]\hbar\omega[a_d,Z]} \sum_{\ell'=-3,5} \times \sum_{N'\neq N} \frac{V_{N,\ell,N'}\,|t^j,\ell'N'\rangle}{2(N-N') + 1 - \sqrt{(\ell-1)^2+1}}, \tag{D2}$$

where $V_{N;\ell,N'} = \langle t^j,1N \mid \tilde{R}^4 \mid t^j,\ell N'\rangle$ is a dimensionless number. These admixtures can have a strong impact on the loss rate, especially for $\ell = 1$, which is lossless to zeroth order as seen from Eq. (24) and Fig. 6, but becomes lossy due to the small admixture of the degenerate states $\ell = -3,5$. It is clear that the correction does not couple different hyperfine manifolds, so we will drop the hyperfine subscript j. From Eq. (D2), we find that the modified decay rate for the $N = 0$ motional state of $\ell = 1$ is given by Eq. (25).

The next source of loss originates from the last term in Eq. (D1), which couples the trapped t_ℓ state to the continuum states $u_{\ell\pm4}$. Using Fermi's golden rule, the loss rate for the $N = 0, \ell = 1$ state consequently is given by Eq. (26).

2. Loss rate for 1D trap

For 1D trap, in the electric field expansion in Eq. (34), both $\exp[\pm i3\phi_q]$ terms are present. As a result, the equivalent of Eq. (D1),

$$\frac{-1}{2}\left(\partial_{\tilde{R}}^2 + \frac{\partial_{\tilde{R}}}{\tilde{R}} - \frac{1}{\tilde{R}^2} - 2\tilde{R}^2\right) t_1^j[\tilde{R}] + \frac{K\tilde{R}^4}{2F_\perp[a_d,Z]\omega[a_d,Z]} \times \sum_{\eta=\pm1}\left(F_{-3}[a_d,Z]t_{1+4\eta}^j[\tilde{R}] + F_3[a_d,Z]t_{1+2\eta}^j[\tilde{R}] + \frac{3}{4}F_{-3}[a_d,Z]u_{1+4\eta}^j[\tilde{R}] + \frac{3}{4}F_3[a_d,Z]u_{1+2\eta}^j[\tilde{R}]\right) = \frac{\epsilon_1 + E_i}{\hbar\omega[a_d,Z]} t_1^j[\tilde{R}]. \tag{D3}$$

Then we get the loss rates for 1D following the same procedure in as the previous subsection.

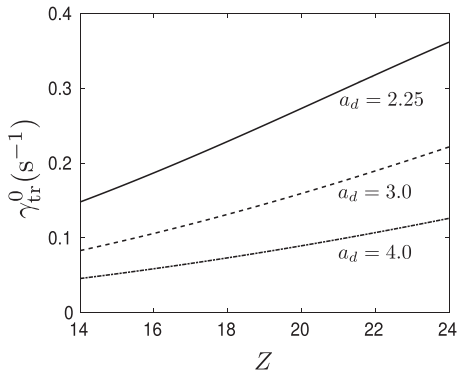

FIG. 8. Total nonadiabatic and hyperfine-induced loss rate $\gamma_{\rm tr}^0$ is plotted as a function of Z for $a_d = 2.25$ (solid line), 3.0 (dashed line), and 4.0 (dash-dotted line).

APPENDIX E: TOTAL MOLECULAR LOSS FOR A DIFFERENT MAGNETIC FIELD

Here we show the total molecular loss rate $\gamma_{\rm tr}$ as defined in Eq. (27) for a magnetic field $B_0 = 5$T. For such a magnetic field, the hyperfine parameters of Eqs. (2) and (3) for the $j = 0,1$ states are given by $\delta \approx 0.01$ and $|E_1 - E_0|/(\hbar B_e) \approx 0.027$. For such parameters, along with the ferroelectric parameter of the 0D trap from Table I, we plot the loss rate for different values of a_d in Fig. 8.

APPENDIX F: EFFECT OF E_Z FIELD

An additional loss channel arises due to the second-order Stark term in Eq. (8),

$$V_Z^{\mathcal{N}=1} = -\frac{E_Z^2[\vec{\rho}]a_{\rm mf}^2}{20\hbar B_e} \sum_{\substack{\mathcal{M}_1=\pm1 \\ \mathcal{I}_{\rm col}}} |1,\mathcal{M}_1,\mathcal{I}_{\rm col}\rangle\langle 1,\mathcal{M}_1,\mathcal{I}_{\rm col}|. \tag{F1}$$

By using the fitting potential of Eq. (10), $E_Z[\vec{\rho}] \approx f_z[a_d,Z]R^2\sin[2\varphi], R \to 0$ and going to the position basis as used for Eq. (15), the transformed equation reads

$$\left[-\partial_{\tilde{R}}^2 - \frac{\partial_{\tilde{R}}}{\tilde{R}} + \frac{(\ell-1)^2+1}{\tilde{R}^2} + \tilde{R}^2 - \frac{f_z^2[a_d,Z]K}{2f_\perp^2[a_d,Z]\hbar\omega[a_d,Z]}\tilde{R}^4\right] t_\ell^j[\tilde{R}] + \frac{f_z^2[a_d,Z]K}{4f_\perp^2[a_d,Z]\hbar\omega[a_d,Z]}\tilde{R}^4\left(t_{\ell+4}^j[\tilde{R}] + t_{\ell-4}^j[\tilde{R}]\right) = \frac{2(\epsilon_\ell + E_j)}{\hbar\omega[a_d,Z]} t_\ell^j[\tilde{R}]. \tag{F2}$$

We solve Eq. (F2) perturbatively with the zeroth-order solution given by Eq. (16). The attractive R^4 will lower the barrier due to the quadratic potential for large R and will lead to tunneling loss. From a semiclassical Wentzel-Kramers-Brillouin approximation, the tunneling loss rate is found to be negligible compared to the other time scales involved in our system and as a result we neglect this effect. The last two terms will perturbatively couple t_1^j to $t_{-3,5}^j$. Again, there is no coupling between different hyperfine j states and as a result we drop the label for rest of the section. The perturbed state is given by

$$|\underline{t}^j,1N\rangle = |t^j,1N\rangle + \frac{f_z^2[a_d,Z]K}{4f_\perp^2[a_d,Z]\hbar\omega[a_d,Z]} \times \sum_{\ell'=-3,5}\sum_{N'\neq N}\frac{V_{N,\ell,N'}\,|t^j,\ell'N'\rangle}{2(N-N')+1-\sqrt{(\ell-1)^2+1}}, \tag{F3}$$

where $V_{N;\ell,N'}$ is defined below Eq. (D2). Such a superposition will have an impact on the loss rate, specially for $\ell = 1$. In the zeroth order, the $\ell = 1$ is the only lossless state as seen from Eq. (24) and Fig. 6. The loss rate is same as Eq. (25) with $\frac{f_{-3}[a_d,Z]}{f_\perp[a_d,Z]}$ replaced by $(\frac{f_z[a_d,Z]}{2f_\perp[a_d,Z]})^2$. We find that $\frac{f_z[a_d,Z]}{f_\perp[a_d,Z]} \sim 10^{-1}$ and the loss rate is $\sim 10^{-2}\mathrm{s}^{-1}$ for $a_d = 2.25, Z = 16$.

APPENDIX G: EFFECT OF COUPLING TO $|\mathcal{N}=1,\mathcal{M}_\mathcal{N}=0\rangle$ STATE

One of the loss channels we have neglected so far is due to the coupling between a $|\pm1\rangle = |\mathcal{N}=1,\mathcal{M}_\mathcal{N}=\pm1\rangle$ and $|0\rangle = |\mathcal{N}=1,\mathcal{M}_\mathcal{N}=0\rangle$ states. Such coupling arises again via quadratic Stark shift and the corresponding coupling Hamiltonian is given by

$$V_{0\perp}^\mathcal{N} = \frac{a_{\mathrm{mf}}^2 E_Z}{\sqrt{2}\hbar B_e}\left(E_+ V_{0+}^\mathcal{N} + E_- V_{0-}^\mathcal{N}\right), \tag{G1}$$

where

$$V_{0+}^\mathcal{N} = \sum_{\epsilon=0,1}\sum_{\mathcal{N}',\mathcal{M}_{\mathcal{N}'}}\frac{\boldsymbol{T}_{\boldsymbol{\epsilon}}^{\mathbf{1}}\,|\mathcal{N}',\mathcal{M}_{\mathcal{N}'}\rangle\,\langle\mathcal{N}',\mathcal{M}_{\mathcal{N}'}|\,\boldsymbol{T}_{\boldsymbol{\epsilon}}^{\mathbf{1}}}{E_\mathcal{N}-E_{\mathcal{N}'}}, \tag{G2}$$

$$V_{0-}^\mathcal{N} = \sum_{\epsilon=0,-1}\sum_{\mathcal{N}',\mathcal{M}_{\mathcal{N}'}}\frac{\boldsymbol{T}_{\boldsymbol{\epsilon}}^{\mathbf{1}}\,|\mathcal{N}',\mathcal{M}_{\mathcal{N}'}\rangle\,\langle\mathcal{N}',\mathcal{M}_{\mathcal{N}'}|\,\boldsymbol{T}_{\boldsymbol{\epsilon}}^{\mathbf{1}}}{E_\mathcal{N}-E_{\mathcal{N}'}}. \tag{G3}$$

For the first rotational level $\mathcal{N}=1$, the internal states are characterized by $|-1\rangle = |\mathcal{N}=1,\mathcal{M}_\mathcal{N}=-1\rangle, |0\rangle = |\mathcal{N}=1,\mathcal{M}_\mathcal{N}=0\rangle, |1\rangle = |\mathcal{N}=1,\mathcal{M}_\mathcal{N}=1\rangle$. With these basis states, the various components of the coupling matrices are given by

$$V_{0+}^1 \approx \begin{bmatrix}0 & 3/20 & 0\\ 0 & 0 & 3/20\\ 0 & 0 & 0\end{bmatrix},\quad V_{0-}^1 \approx \begin{bmatrix}0 & 0 & 0\\ 3/20 & 0 & 0\\ 0 & 3/20 & 0\end{bmatrix}.$$

By including the energy shift of the $|0\rangle$ state due to laser potential, $E_0 = -\alpha_0 I_0$ [33], and using Fermi's golden rule, the loss rate is proportional to the coupling constant, $|\langle t;\ell;N;\mathcal{N}=1|\,V_{0\perp}^\mathcal{N}\,|0,\vec{k}\rangle|^2$, where $|0,\vec{k}\rangle = e^{i\vec{k}\cdot\vec{R}}\,|0\rangle/\sqrt{A}$ is a 2D free particle state with momentum $\vec{k}$, $|\vec{k}| = \sqrt{(\epsilon_{\ell,N}[Z]+E_0)/K}$. We find that specifically for the $\ell = 1$ state, i.e., the state $|t;\ell=1;N;\mathcal{N}=1\rangle$, the above integral vanishes, i.e., $|\langle t;\ell=1;N;\mathcal{N}=1|\,V_{0\perp}^\mathcal{N}\,|0,k\rangle| = 0$ as $E_Z \propto \sin 2\varphi$ [Fig. 1(c)].

APPENDIX H: EFFECT OF CASIMIR-POLDER FORCE

Another possible modification arises from attractive Casimir-Polder potential. Using similar effective medium arguments, we can infer that the important contribution comes from the substrate. For a planar substrate in the nonretarded regime, from Ref. [49] we can write down the Casimir-Polder potential for the level $|\mathcal{N}=1,\mathcal{M}_\mathcal{N}=\pm1\rangle$ as

$$V_{\mathrm{Casimir}} = -\frac{3\mu^2}{160\pi\epsilon_0}\frac{\epsilon_s-1}{\epsilon_s+1}\frac{1}{Z^3},$$

where Z is the distance (not scaled with r_d) and ϵ_s is the static dielectric constant of the substrate ($\epsilon_s \gg 1$). As we trap our molecule at a distance of $Z_0 \approx 420$ nm from the substrate, the strength of the Casimir-Polder energy for RbCs molecule is $V_{\mathrm{Casimir}}/\hbar B_e \approx 10^{-7} \ll \hbar\omega[Z_0]$, much weaker than the trapping potential.

APPENDIX I: EXPANSION OF $E_-[m_x,m_y;\vec{R},Z]$ IN EQ. (7) AND THE RESULTING TOTAL AZIMUTHAL FIELD $E_-[\vec{\rho}]$

To look for the behavior of the electric field, we first chose a rectangular configuration from Fig. 1(b) with the nanorod positions, $[m_x(qa_{\mathrm{latt}}-a_d), m_y a_d]$ and for a fixed q and $m_x = \pm1, m_y = \pm1$. The electric field for such a configuration can be written as

$$E_-[q,\boldsymbol{m};\vec{\rho}] = -(-1)^{\frac{m_x+m_y}{2}}e^{-i\tilde{\phi}_{q,\boldsymbol{m}}}\int d\vec{r}(E[Z+h]-E[Z]) \times (R_{q,\boldsymbol{m}} - re^{-i(\phi-\phi_{q,\boldsymbol{m}})}),$$
$$E[Z] = (Z^2+|\vec{R}_{q,\vec{m}}-\vec{r}|^2)^{-3/2}, \tag{I1}$$

where $\vec{R}_{q,\boldsymbol{m}} = \vec{R} - \vec{F}_{q,\boldsymbol{m}}$, $\boldsymbol{m} \equiv (m_x,m_y)$, and $\tan\phi_{q,\boldsymbol{m}} = (Y - m_y a_d)/[X - m_x(qa_{\mathrm{latt}}-a_d)]$. The total field components are given as the sum of the contributions of all nanorods by $E_{-q}[\vec{\rho}]$:

$$E_{-q}[\vec{\rho}] = \sum_{\boldsymbol{m}} E_-[q,\boldsymbol{m};\vec{\rho}]. \tag{I2}$$

1. Terms of order R

As we are interested in the field near the center of the rectangle, we carry out the integration over r in Eq. (I1) and we expand the resulting expression as a function of $R \ll a_d/2$. The electric field can be written as

$$E_-[q,\boldsymbol{m};\vec{\rho}] = (-1)^{\frac{m_x+m_y}{2}}s_{m_x,m_y}e^{-i\tilde{s}_{m_x,m_y}\phi_0} \times \left(1+i\{m_x a_x Y - m_y a_d X\} + O\left[R_q^2\right]\right) \times \left(g_0[R_q,Z] + g_1[R_q,Z]\{m_x a_x X + m_y a_d Y\} + O\left[R_q^2,Z\right]\right), \tag{I3}$$

where we have defined $a_x = qa_{\mathrm{latt}} - a_d$ and $R_q^2 = a_x^2 + a_d^2$ and $g_{0,1}[R_q]$ are functions resulting from the integration which only depends on R_q and Z. Moreover, we define the angle $\tan\phi_0 = (a_d/a_x)$. The sign functions are defined as $s_{1,1} = s_{1,-1} = 1; s_{-1,1} = s_{-1,-1} = -1$ and $\tilde{s}_{1,1} = \tilde{s}_{-1,-1} = 1; \tilde{s}_{-1,1} = \tilde{s}_{1,-1} = -1$. Now from Eqs. (I3) and (I2), by

carrying out the summation for terms $\propto R$, we find that $E_{-q}[\vec{\rho}] \propto Re^{i\phi}$. As a result, to get the full electric field, one sums over terms similar to Eq. (I2) over different q which only changes the strength of the leading-order term.

APPENDIX J: DERIVATION OF SIMULATION HAMILTONIAN

Here we derive the equation in Eq. (41). At first, we only consider a single molecule near the ferroelectric substrate in a linearly Z-polarized microwave field $\vec{E}_{\rm mw} = E_0 \cos\Omega t\,\hat{Z}$, where $\Omega = 4B_e + \Delta$ with $\Delta \ll B_e$. Such a frequency will resonantly couple $|\mathcal{N}=1\rangle$ to $|\mathcal{N}=2\rangle$ state. Our Hamiltonian is then given by

$$H = \sum_{\mathcal{N},\mathcal{M}_\mathcal{N}} E_\mathcal{N} |\mathcal{N},\mathcal{M}_\mathcal{N}\rangle \langle\mathcal{N},\mathcal{M}_\mathcal{N}| + \sum_{\substack{|\mathcal{N}-\mathcal{N}'|=1,\\ \mathcal{M}_\mathcal{N},\mathcal{M}'_\mathcal{N}}} H_{\rm mf}[\mathcal{N}',\mathcal{M}'_\mathcal{N};\mathcal{N},\mathcal{M}_\mathcal{N}] |\mathcal{N}',\mathcal{M}'_\mathcal{N}\rangle \langle\mathcal{N},\mathcal{M}_\mathcal{N}|$$
$$+ \cos\Omega t \sum_{\substack{|\mathcal{N}-\mathcal{N}'|=1,\\ \mathcal{M}_\mathcal{N}}} g_{\rm mw}[\mathcal{N}',\mathcal{N},\mathcal{M}_\mathcal{N}] |\mathcal{N}',\mathcal{M}_\mathcal{N}\rangle \langle\mathcal{N},\mathcal{M}_\mathcal{N}|\,, \tag{J1}$$

where the molecular rotational energy $E_\mathcal{N} = \hbar B_e \mathcal{N}(\mathcal{N}+1)$ and the molecule-ferroelectric coupling $H_{\rm mf}[\mathcal{N}',\mathcal{M}'_\mathcal{N};\mathcal{N},\mathcal{M}_\mathcal{N}] = \langle\mathcal{N}',\mathcal{M}'_\mathcal{N}| H_{\rm mf} |\mathcal{N},\mathcal{M}_\mathcal{N}\rangle$ with $H_{\rm mf}$ are defined in Eq. (5) and are position dependent. The microwave coupling is given by $g_{\rm mw}[\mathcal{N}',\mathcal{N},\mathcal{M}_\mathcal{N}] = \mu E_0 \langle\mathcal{N}',\mathcal{M}_\mathcal{N}| \boldsymbol{T_0^1} |\mathcal{N},\mathcal{M}_\mathcal{N}\rangle$. We apply the unitary transformation, $\boldsymbol{U}_t = \exp[-i\sum_{\mathcal{N},\mathcal{M}_\mathcal{N}} E_\mathcal{N} |\mathcal{N},\mathcal{M}_\mathcal{N}\rangle \langle\mathcal{N},\mathcal{M}_\mathcal{N}|\,t]$, and carry out the transformation $H' = \boldsymbol{U}^{\dagger_t} H \boldsymbol{U}_t - i\boldsymbol{U}_t^\dagger[d_t \boldsymbol{U}_t]$. As a result, Eq. (J1) becomes

$$H' = \Delta \sum_{\mathcal{M}_2} |2,\mathcal{M}_2\rangle \langle 2,\mathcal{M}_2| + \frac{1}{2}\sum_{\mathcal{M}_1}(g_{\rm mw}[2,1,\mathcal{M}_1] |2,\mathcal{M}_1\rangle \langle 1,\mathcal{M}_1| + g_{\rm mw}[1,2,\mathcal{M}_1] |1,\mathcal{M}_1\rangle \langle 2,\mathcal{M}_1|)$$
$$+ \sum_{\substack{|\mathcal{N}-\mathcal{N}'|=1,\\ \mathcal{M}_\mathcal{N},\mathcal{M}'_\mathcal{N}}} H_{\rm mf}[\mathcal{N}',\mathcal{M}'_\mathcal{N};\mathcal{N},\mathcal{M}_\mathcal{N}] \exp[i(E_{\mathcal{N}'} - E_\mathcal{N})t] |\mathcal{N}',\mathcal{M}'_\mathcal{N}\rangle \langle\mathcal{N},\mathcal{M}_\mathcal{N}|$$
$$+ \frac{1}{2}\sum_{\mathcal{M}_1}(g_{\rm mw}[2,1,\mathcal{M}_1] e^{i8B_e t} |2,\mathcal{M}_1\rangle \langle 1,\mathcal{M}_1| + g_{\rm mw}[1,2,\mathcal{M}_1] e^{-i8B_e t} |1,\mathcal{M}_1\rangle \langle 2,\mathcal{M}_1|)$$
$$+ \cos\Omega t \sum_{\substack{|\mathcal{N}-\mathcal{N}'|=1,\\ \mathcal{M}_\mathcal{N}}}{}' g_{\rm mw}[\mathcal{N}',\mathcal{N},\mathcal{M}_\mathcal{N}] \exp[i(E_{\mathcal{N}'} - E_\mathcal{N})t] |\mathcal{N}',\mathcal{M}_\mathcal{N}\rangle \langle\mathcal{N},\mathcal{M}_\mathcal{N}|, \tag{J2}$$

where in the first line we have defined the time-independent component in the transformed Hamiltonian and in the last line the summation $\sum'$ excludes transitions between $\mathcal{N}=1$ and $\mathcal{N}=2$ states. We carry out a Floquet-Magnus expansion [50] up to second order $(1/\Omega^2)$, which results in the effective Hamiltonian in the $\mathcal{N}=1,2$ subspace

$$H_{\rm eff} = \Delta \sum_{\mathcal{M}=-2}^{2} |2,\mathcal{M}\rangle \langle 2,\mathcal{M}| + g \sum_{\mathcal{M}=\pm1} (|2,\mathcal{M}\rangle \langle 1,\mathcal{M}| + h.c.) + g\sqrt{2/3}(|2,0\rangle \langle 1,0| + \text{H.c.})$$
$$+ \sum_{\mathcal{M}'_1,\mathcal{M}_1} V^1[\mathcal{M}'_1,\mathcal{M}_1] |1,\mathcal{M}'_1\rangle \langle 1,\mathcal{M}_1| + \sum_{\mathcal{M}_2,\mathcal{M}'_2} V^2[\mathcal{M}'_2,\mathcal{M}_2] |2,\mathcal{M}'_2\rangle \langle 2,\mathcal{M}_2|\,, \tag{J3}$$

where the matrix elements in $V^\mathcal{N}$ are given by Eq. (8) and $g = \mu E_0/\sqrt{20}$. The first line represents the time-independent part and the second line comes from the first term in the Magnus expansion [50]. As we noticed from our discussion of Eqs. (8), the terms of the last line will give rise to trapped states $|t;\mathcal{N}=1\rangle$ and $|t;\mathcal{N}=2\rangle$ with energy $\hbar\omega[Z_1]$ and $\hbar\omega[Z_2]$. Then, if we project the Hamiltonian in Eq. (J3) to the motional ground states in the two $\mathcal{N}$ subspaces and define the operators $\boldsymbol{S}^+ = |t;\mathcal{N}=1\rangle \langle t;\mathcal{N}=1|\,, \boldsymbol{S}^z = |t;\mathcal{N}=2\rangle \langle t;\mathcal{N}=2| - |t;\mathcal{N}=1\rangle \langle t;\mathcal{N}=1|$, and $\boldsymbol{S}^- = [\boldsymbol{S}^+]^\dagger$, this gives rise to the last two terms in Eq. (41), where we have introduced an additional subscript q to denote the mean position of the trapped state. Next, we look into the situation when each site in the periodic potential is filled with one molecule and consider the effects of the dipolar interaction. Dipolar interaction between the two molecules is given by

$$V_{\rm dip} = \frac{\boldsymbol{\mu}_1 \cdot \boldsymbol{\mu}_2 - 3(\boldsymbol{\mu_1} \cdot \hat{\rho}_{12})(\boldsymbol{\mu_2} \cdot \hat{\rho}_{12})}{|\vec{\rho}_{12}|^3}, \tag{J4}$$

where $\boldsymbol{\mu}_{1,2}$ are the dipole moment operators for molecules are position $\vec{\rho}_{1,2}$ and $\vec{\rho}_{12} = \vec{\rho}_1 - \vec{\rho}_2$. Between molecules at sites q and q', the resonant dipolar interaction is given by

$$\langle t;\mathcal{N}=2|_q \langle t;\mathcal{N}=1|_{q'} V_{\rm dip} |t;\mathcal{N}=1\rangle_q |t;\mathcal{N}=2\rangle_{q'} = \sum_{\mathcal{M}_\mathcal{N}=\pm1} \frac{\mu^2 |\langle\mathcal{N}=2,\mathcal{M}_\mathcal{N}|\boldsymbol{T_0^1}|\mathcal{N}=1,\mathcal{M}_\mathcal{N}\rangle|^2}{16\pi\epsilon_0 |q-q'|^3 a_d^3}, \tag{J5}$$

where we assume that $1 \gg \sigma[a_d, Z]/a_d$ and give rise to the first term in Eq. (41). There will also be losses due to dipolar coupling of untrapped state. After some algebra, one such lossy term can be written as

$$\begin{aligned}
&\langle \mathcal{N}=2, \mathcal{M}_\mathcal{N}=0; k| \langle \mathcal{N}=1, \mathcal{M}_\mathcal{N}=0; k'| V_{\rm dip} |t; \mathcal{N}=1\rangle_q |t; \mathcal{N}=2, -\rangle_{q'} \\
&\approx -\frac{\mu^2 |\exp[-\tilde{R}^2/2 - i\varphi - i\vec{k}\cdot\vec{\tilde{R}}] d^2\tilde{R}|^2}{8\pi\epsilon_0 |q-q'|^3 a_d^3} \langle \mathcal{N}=2, \mathcal{M}_\mathcal{N}=0| \boldsymbol{T}^{\mathbf{1}}_{\mathbf{-1}} |\mathcal{N}=1, \mathcal{M}_\mathcal{N}=1\rangle \\
&\quad \times \langle \mathcal{N}=1, \mathcal{M}_\mathcal{N}=0| \boldsymbol{T}^{\mathbf{1}}_{\mathbf{-1}} |\mathcal{N}=2, \mathcal{M}_\mathcal{N}=1\rangle \\
&\propto \exp[-k^2/4] = \exp\left[-\frac{\alpha_0 I_0}{4K}\right],
\end{aligned} \tag{J6}$$

where we have used for the untrapped state $\langle \mathcal{N}=2, \mathcal{M}_\mathcal{N}=0; k| = \langle \mathcal{N}=2, \mathcal{M}_\mathcal{N}=0| \exp[-i\vec{k}\cdot\vec{\tilde{R}}]$ and $1 \gg \sigma[a_d, Z]/a_d$. For the last line, we have used the fact that due to laser light, the $\mathcal{M}_\mathcal{N}=0$ state is shifted by $\alpha_0 I_0$ (see Sec. V A), and the resonant condition reads $k^2 = \alpha_0 I_0/K$. As a result, the loss rate will be $\propto \exp[-\frac{\alpha_0 I_0}{2K}]$.

[1] M. Lewenstein, A. Sanpera, and V. Ahufinger, *Ultracold Atoms in Optical Lattices: Simulating Quantum Many-Body Systems* (Oxford University Press, Oxford, UK, 2012).

[2] D. E. Chang, K. Sinha, J. M. Taylor, and H. J. Kimble, Nat. Commun. **5**, 4343 (2014).

[3] A. González-Tudela, C.-L. Hung, D. E. Chang, J. I. Cirac, and H. J. Kimble, Nat. Photonics **9**, 320 (2015).

[4] D. DeMille, Phys. Rev. Lett. **88**, 067901 (2002).

[5] S. F. Yelin, K. Kirby, and R. Côté, Phys. Rev. A **74**, 050301 (2006).

[6] H. P. Büchler, E. Demler, M. D. Lukin, A. Micheli, N. Prokof'ev, G. Pupillo, and P. Zoller, Phys. Rev. Lett. **98**, 060404 (2007).

[7] O. Dutta, M. Gajda, P. Hauke, M. Lewenstein, D.-S. Lühmann, B. A. Malomed, T. Sowiński, and J. Zakrzewski, Rep. Prog. Phys. **78**, 066001 (2015).

[8] G. Pupillo, A. Micheli, H. P. Büchler, and P. Zoller, in *Cold Molecules: Theory, Experiment, Applications*, edited by R. Krems, B. Friedrich, and W. C. Stwalley (CRC Press, Boca Raton, FL, 2009), Chap. 12.

[9] L. D. Carr, D. DeMille, R. V. Krems, and J. Ye, New. J. Phys. **11**, 055049 (2009).

[10] J. L. Bohn, A. M. Rey, and J. Ye, Science **357**, 1002 (2017).

[11] M. Pospelov and A. Ritz, Ann. Phys. **318**, 119 (2005).

[12] M. Mayle, G. Quéméner, B. P. Ruzic, and J. L. Bohn, Phys. Rev. A **87**, 012709 (2013).

[13] A. Chotia, B. Neyenhuis, S. A. Moses, B. Yan, J. P. Covey, M. Foss-Feig, A. M. Rey, D. S. Jin, and J. Ye, Phys. Rev. Lett. **108**, 080405 (2012).

[14] L. Reichsöllner, A. Schindewolf, T. Takekoshi, R. Grimm, and H.-C. Nägerl, Phys. Rev. Lett. **118**, 073201 (2017).

[15] V. Fridkin and S. Ducharme, *Ferroelectricity at the Nanoscale: Basics and Applications*, Nanoscience and Technology (Springer-Verlag, Berlin, 2014).

[16] A. N. Morozovska, E. A. Eliseev, and M. D. Glinchuk, Phys. Rev. B **73**, 214106 (2006).

[17] G. Geneste, E. Bousquet, J. Junquera, and P. Ghosez, App. Phys. Lett. **88**, 112906 (2006).

[18] J. M. Wesselinowa, T. Michael, and S. Trimper, in *Handbook of Physics: Nanoparticles and Quantum Dots.*, edited by K. D. Sattler (CRC Press, Boca Raton, FL, 2010).

[19] Z. Hu, M. Tian, B. Nysten, and A. M. Jonas, Nat. Materials **8**, 62 (2009).

[20] D. Guo, F. Zeng, and B. Dkhil, J. Nanosci. Nanotech. **14**, 2086 (2014).

[21] M.-C. García-Gutiérrez, A. Linares, J. J. Hernández, D. R. Rueda, T. A. Ezquerra, P. Poza, and R. J. Davies, Nano Lett. **10**, 1472 (2010).

[22] Y.-Y. Choi, T. G. Yun, N. Qaiser, H. Paik, H. S. Roh, J. Hong, S. Hong, S. M. Han, and K. No, Sci. Rep. **5**, 10728 (2015).

[23] Y. Luo, I. Szafraniak, N. D. Zakharov, V. Nagarajan, M. Steinhart, R. B. Wehrspohn, J. H. Wendorff, R. Ramesh, and M. Alexe, Appl. Phys. Lett. **83**, 440 (2003).

[24] M. Algueró, J. M. Gregg, and L. Mitoseriu, editors, *Nanoscale Ferroelectrics and Multiferroics: Key Processing and Characterization Issues and Nanoscale Effects,* Vol. 1 (John Wiley and Sons, Sussex, UK, 2016).

[25] W. Lee, H. Han, A. Lotnyk, M. A. Schubert, S. Senz, M. Alexe, D. Hesse, S. Baik, and U. Gosele, Nat. Nano. **3**, 402 (2008).

[26] Y. Ahn and J. Y. Son, Organ. Electron. **41**, 205 (2017).

[27] W. J. Chen, Y. Zheng, W. M. Xiong, X. Feng, B. Wang, and Y. Wang, Sci. Rep. **4**, 5339 (2014).

[28] S. Y. T. van de Meerakker, H. L. Bethlem, N. Vanhaecke, and G. Meijer, Chem. Rev. **112**, 4828 (2012).

[29] M. Lara, B. L. Lev, and J. L. Bohn, Phys. Rev. A **78**, 033433 (2008).

[30] J. M. Brown and A. Carrington, *Rotational Spectroscopy of Diatomic Molecules*, 1st ed. (Cambridge University Press, Cambridge, UK, 2003).

[31] P. D. Gregory, J. Aldegunde, J. M. Hutson, and S. L. Cornish, Phys. Rev. A **94**, 041403 (2016).

[32] P. K. Molony, P. D. Gregory, Z. Ji, B. Lu, M. P. Köppinger, C. R. Le Sueur, C. L. Blackley, J. M. Hutson, and S. L. Cornish, Phys. Rev. Lett. **113**, 255301 (2014).

[33] B. Neyenhuis, B. Yan, S. A. Moses, J. P. Covey, A. Chotia, A. Petrov, S. Kotochigova, J. Ye, and D. S. Jin, Phys. Rev. Lett. **109**, 230403 (2012).

[34] R. Halir, P. J. Bock, P. Cheben, A. Ortega-Moñux, C. Alonso-Ramos, J. H. Schmid, J. Lapointe, D.-X. Xu, J. G. Wangüemert-Pérez, I. Molina-Fernández, and S. Janz, Las. Phot. Rev. **9**, 25 (2015).

[35] L. Novotny and B. Hecht, *Principles of Nano-optics*, 2nd ed. (Cambridge University Press, Cambridge, UK, 2012).

[36] C. Sheppard, App. Opt. **52**, 538 (2013).

[37] S. Kotochigova and E. Tiesinga, Phys. Rev. A **73**, 041405 (2006).

[38] S. Kotochigova and D. DeMille, Phys. Rev. A **82**, 063421 (2010).
[39] P. Lalanne and D. Lemercier-Lalanne, J. Opt. Soc. Am. A **14**, 450 (1997).
[40] S. Y. Buhmann, M. R. Tarbutt, S. Scheel, and E. A. Hinds, Phys. Rev. A **78**, 052901 (2008). Note: We have used Eqs. (52), (80), and (82) of this paper and projected into our molecular state to arrive at the expression Eq. (28) in the present paper.
[41] M. G. W. Zeppenfeld, Ph.D. thesis, TU München, Germany, 2013.
[42] L. Li, Y. Fang, Q. Xiao, Y. J. Wu, N. Wang, and X. M. Chen, Int. J. Appl. Ceram. Technol. **11**, 193 (2014).
[43] J. M. Wylie and J. E. Sipe, Phys. Rev. A **30**, 1185 (1984).
[44] I. Naumov, L. Bellaiche, and H. Fu, Nature (London) **432**, 737 (2004).
[45] S. Prosandeev, I. Ponomareva, I. Kornev, and L. Bellaiche, Phys. Rev. Lett. **100**, 047201 (2008).
[46] M. Goiriena-Goikoetxea, A. García-Arribas, M. Rouco, A. V. Svalov, and J. M. Barandiaran, Nanotech. **27**, 175302 (2016).
[47] Q. F. Xiao, J. Rudge, B. C. Choi, Y. K. Hong, and G. Donohoe, Appl. Phys. Lett. **89**, 262507 (2006).
[48] J. D. Joannopoulos, S. G. Johnson, J. N. Winn, and R. D. Meade, *Photonic Crystals* (Princeton University Press, Princeton, NJ, 2008).
[49] G. Bimonte, T. Emig, R. L. Jaffe, and M. Kardar, Phys. Rev. A **94**, 022509 (2016).
[50] E. S. Mananga and T. Charpentier, J. Chem. Phys. **135**, 044109 (2011).